Portland State University

PDXScholar

Dissertations and Theses

Dissertations and Theses

Winter 3-4-2013

Use of Soybean Lecithin in Shape Controlled Synthesis of Gold Nanoparticles

Benjamin Robert Ayres
Portland State University

Follow this and additional works at: https://pdxscholar.library.pdx.edu/open_access_etds

 Part of the Physical Chemistry Commons

Let us know how access to this document benefits you.

Recommended Citation

Ayres, Benjamin Robert, "Use of Soybean Lecithin in Shape Controlled Synthesis of Gold Nanoparticles" (2013). *Dissertations and Theses.* Paper 628.
https://doi.org/10.15760/etd.628

This Dissertation is brought to you for free and open access. It has been accepted for inclusion in Dissertations and Theses by an authorized administrator of PDXScholar. Please contact us if we can make this document more accessible: pdxscholar@pdx.edu.

Use of Soybean Lecithin in Shape Controlled Synthesis of Gold Nanoparticles

by

Benjamin Robert Ayres

A dissertation submitted in partial fulfillment of the
requirements for the degree of

Doctor of Philosophy
in
Chemistry

Dissertation Committee:
Dean Atkinson, Chair
Scott M. Reed
Shankar Rananavare
Andrea Goforth
Jon Abramson
Susan Masta

Portland State University
2013

Abstract

The work presented in this dissertation is a composite of experiments in the growth of gold nanoparticles with specific optical properties of interest. The goal is to synthesize these gold nanoparticles using soybean extract for not only shape control, but for propensity as a biocompatible delivery system.

The optical properties of these nanoparticles has found great application in coloring glass during the Roman empire and, over the centuries, has grown into its own research field in applications of nanoparticulate materials. Many of the current functions include use in biological systems as biosensors and therapeutic applications, thus making biocompatibility a necessity. Current use of cetyltrimethylammonium bromide leads to rod-shaped gold nanoparticles, however, the stability of these gold nanoparticles does not endure for extended periods of time in aqueous media.

In my research, two important components were found to be necessary for stable, anisotropic growth of gold nanoparticles. In the first experiments, it was found that bromide played a key role in shape control. Bromide exchange on the gold atoms led to specific packing of the growing crystals, allowing for two-dimensional growth of gold nanoparticles. It was also discerned that soybean lecithin contained ligands that blocked specific gold facets leading to prismatic gold nanoparticle growth. These gold nanoprisms give a near infrared plasmon absorption similar to that of rod-shaped gold nanoparticles. These gold nanoprisms are discovered to be extremely stable in aqueous media and remain soluble for extended periods of time, far longer than that of gold nanoparticles grown using cetyltrimethylammonium bromide.

Since soy lecithin has a plethora of compounds present, it became necessary to discover which compound was responsible for the shape control of the gold nanoprisms in order to optimize the synthesis and allow for a maximum yield of the gold nanoprisms. Many of these components were identified by high performance liquid chromatography and liquid

chromatography–mass spectrometry. However, re-spike of these components into growth solutions did not enhance the growth of gold nanoprisms.

Upon separating the shapes of the gold nanoparticles using gel electrophoresis, addition of KCN to the separated gold nanoparticles allowed us to extract the culpable ligands for shape control. Analysis of these ligands by mass spectrometry elucidated the identity of PA and upon re-spike of the PA into a growth solution of PC_{95}, the growth of a near-infrared plasmon absorption was seen.

The stability of these gold nanoparticles was tested with and without the addition of decane thiol and it was concluded that addition of the thiol allowed for improved stability of the gold nanoparticles towards cyanide. It was determined that at a concentration of 2 μM decanethiol, spherical gold nanoparticles remained stable to cyanide at the expense of the prismatic gold nanoparticles. However, at 5 μM decanethiol, both spherical and prismatic gold nanoparticles retained stability to cyanide in aqueous conditions.

Acknowledgements

I would begin by acknowledging my principle investigator, Scott Reed. There is no question that his support and trust have allowed me to reach this goal in my life. He left Portland three years ago to pursue his own goals as a professor, a husband and a father, however he continued to support and guide me in my endeavor in this achievement. In allowing me to continue my work independently, he has shown confidence in my ability as a scientist and this has allowed me to grow in self-reliance and aptitude. My sincere appreciation goes to Marilyn Mackiewicz for providing guidance and friendship and helping see me through the good and the bad. I am also immensely thankful to John Yan, Brian Larson and the other graduate students who have helped to keep me sane with their friendship and jovial dispositions. A special thanks to Joan Zivi and Sinnamon Tearny, who have been especially helpful in guiding me in my graduate requirements and helping keep my financial support.

A very grateful thank you my committee members for their patience and flexibility through all the steps of my graduate career. Their advice and criticism throughout my graduate career has been invaluable in this achievement and I sincerely appreciate all the help and time they have given me. I'd especially like to thank those faculty and staff that allowed me time on their instruments without which I would never have completed the research.

Finally, I would like to express my love and gratitude to Kacie, my mother and father, my brothers, Mike and Josh, and the rest of my family. Without your love and support over the years, I would never have achieved this goal. Your dedication, belief and

encouragement have allowed me to finish this momentous chapter in my life and I am forever grateful to you. I will continue to make you proud and strive to do my best in everything I do.

Table of Contents

List of Figures

List of Abbreviations

CTAB – cetyltrimethylammonium bromide

GNPs – Gold nanoparticles

FWHM – Full width half maximum

HPLC – high performance liquid chromatography

LC-MS – liquid chromatography – mass spectrometry

MS – mass spectrometry

PC - phosphatidylcholine

PE – phosphatidylethanolamine

PC_{30} – Soy extract containing 30% phosphatidylcholine

PC_{95} – Soy extract purified to contain 95% phosphatidylcholine

TBE – tris boric acid ethylenediamine buffer

TEM – transmission electron microscopy

TLC – thin layer chromatography

UV-Vis – UV-visible spectrometry

Introduction

1.1 – Gold nanoparticles in medicine

Gold has been used since ancient times in a plethora of applications, from early uses in glass staining and as a monetary base, to more recent applications in microcomputing and medicine.[1-18] The advancements of gold have been tracked as far back as 5000 B.C. for use in jewelry and art. As the properties of the metal were explored, gold became a popular use for potions and medicine.[19] It was believed to contain magical qualities and its likeness to the sun made gold led to a reverent use of gold by priests, healers and shaman. Wiegleb documented some of the earliest uses of gold as medicine in Chinese culture as far back as 2500 B.C.[20] another well documented account was of Moses burning the golden calf, preparing a potion from the ashes, and forcing the Children of Israel to "… drink of it", is probably one of the earliest accounts of the practice of alchemy involving gold.[21] The Taoist philosophers of ancient China used gold and silver coatings on medications to hopefully enhance the quality of their potions in 600 B.C.[22,23] Both Pliny the Elder and Dioscorides, in the first century A.D., record the use of gold as a medicinal agent.[24] The great Persian medical schools, initiated by the Nestorian Christians, write that the pharmacist-physicians Yabir, Avicenna and Rhazes all supported the use of gold compounds as a panaceae. Yabir is attributed to have discovered the formulation of aqua-regia, capable of dissolving elemental gold. Medical knowledge from these Arab based sites of learning eventually spread into Europe and the British Isles. Philippus Aureleos Paracelsus, considered by some as the founder of

modern therapeutics, is reputed to have first used gold compounds in the treatment of tuberculosis and advocated the use of gold as a cure-all.

It wasn't until the early 19th century that the work of Andre-Jean Chrestien and Pierre Figuier, two professors at the University of Montpellier, laid the groundwork for modern use of gold compounds in medicine.[25] Figuier was a pharmacist who put forth the formulations for gold salts such as gold sodium chloride. Chrestien then used this as a treatment of tuberculosis and syphilis in his 1811 publication, De La Methode Intraleptique. Soon after Chrestien's work, the nobel laureate Dr. Robert Koch discovered that gold cyanide was bactericidal in vitro to tubercle bacilli.[26] An erroneous but lucky assumption by Dr. Jacques Forestier that rheumatoid disease was an infectious disease analogous to tuberculosis led him to use gold thiopropanol sodium sulphonate on 15 patients with inflammatory rheumatoid disease.[27] The successful clinical experiment led researchers over the next 70 years to investigate both the beneficial and the toxic effects of anti-arthritic gold complexes.

More recent advances in gold therapy have led to potential use of gold nanoparticles (GNPs) in cancer treatment.[19,28-37] In many applications of GNPs in therapy, their optical properties are responsible for the therapeutic effects. GNP's characteristic optical properties can be manipulated by controlling the shape of the GNP. For instance, in the case of rod shaped GNPs,[29,31,37] two plasmon absorptions are seen in the UV-Visible spectrometer. The same can be seen in prismatic GNPs.[38] Gold "nanoshells" have a long wavelength absorption.[39] In these cases, the wavelength absorption in the near infrared

(NIR) emits heat as energy. Using this heat, it has been proposed that GNPs can be functionalized to target tumors and the tumors can be treated via hyperthermia.[31,38,40,41] Extensive research has been performed to synthesize biocompatible GNPs, which have absorption peaks in the NIR. These optical properties have been studied extensively for centuries.

1.2 – Mechanisms in gold colloid synthesis

Anisotropic noble metal nanoparticles have recently found great use in electronics, catalysis and medicinal applications.[42-49] The optical and physical properties from their size and shape give these nanoparticles widespread applications in these areas. The synthetic groundwork of noble metal nanoparticles to control their size and shape has been studied extensively. Arguably, the largest challenge to these syntheses has been shape control, particularly for GNPs. Shape controlled synthesis of GNPs is dependent on many factors such as seed mediation, gold source and surface ligand selection. Many factors leading to shape control have been studied such as halide addition, silver assisted synthesis, temperature dependence and seed morphology. Seed-mediated synthesis in particular has led to many shapes such as rods, prisms, cubes, octahedra and plates. It was found that addition of ions added to these growth solutions can be used to adjust the shape control.

Some of the first successful experiments done in shape control were performed in 1996 when gold nanoparticles were grown by eletrodeposition in porous aluminum oxide. The

resulting rods showed interesting optical properties in the Visible-near-infrared spectra. Concurrent research found that electrochemical growth of gold nanorods was easily achieved using an oxidation/reduction method in a two-electrode cell (Pt/Au) when the reaction was done in an aqueous CTAB solution.[50] A fairly uniform solution of rods formed and the aspect ratio could be manipulated by changing the reaction conditions. Further research into this method found that as the solution temperature increased, the aspect ratio decreased, giving another method of manipulating shape and size of gold nanorods.[51]

Although the electrochemical method was effective, new research went into finding a synthetic method to control shape. A seed-mediated synthesis was found to be the most effective method of shape control of GNPs.[52] For anisotropic shapes from the more ordinary rod and prismatic shaped nanoparticles to the more exotic periwinkle and star-shaped nanoparticles, seed-mediated methods are employed.[44,53,54] The morphology of the seed was found to be important in the resulting GNP growth.[55] It has been found that different morphologies of rod-shaped GNPs resulted depending on if the seed was single crystalline or multiply twinned. Seeds with pentatwinned morphology result in twinned gold nanorods as well as twinned bipyramidal nanoparticles while the single crystalline seeds result in single crystalline gold nanorods.[55,56]

Seed size has also been shown to affect GNP morphology.[57] The seeds are believed to provide nucleation points for growth of larger particles and the reactivity of smaller particles allows for larger growth effects. The smaller seeds also allow for more

variability in growth features such as concavity and available facets. Larger seeds (>15 nm) contain larger facets for gold deposition to occur resulting in poor shape control.

Ion doping also has been found to affect GNP morphology. Multiple groups have studied the catalytic effect of silver ions in the growth solution originally investigated by El-Sayed.[55,56,58] This was reported as an underpotential deposition of Ag(I) which leads a strong influence of ordering the ions on the more open (110) face of the crystal. Iodide spiking has also been found to change the resulting crystal shape in GNPs.[38,59,60,61,62] As discussed, silver adsorbs selectively to {110} Au facets by underpotential deposition (UPD) and inhibits Au deposition on those surfaces but allows Au deposition on {100} and {111} surfaces, leading to nanorod growth in the [100] direction. However, iodide has a higher propensity to Au {111} surfaces and prevents nanorod growth by blocking that surface. By manipulating the concentration of iodode present in growth solutions, prism, dogbone and ellipsoid shapes can result.[61,62]

Other factors affecting shape control of GNPs can be pH[63] and heat.[62] Varying the pH of a growth solution has been found to affect micelle growth. At low pH, ionic moieties are protonated and change the intermolecular binding energies causing a different growth pattern. Also, a higher pH results in negative charge building on the GNP surface, thereby increasing electrostatic repulsion. As a result, nanoparticle fusion is efficiently inhibited giving a single modal growth of GNPs. pH effects lead to shapes such as needle-like nanoparticles, spherical nanoparticles and nanorods. As to heat effects, heat has been attributed to increased width of gold nanorods. Heating growth solutions to 100

^{o}C found that the resulting rods had reduced aspect ratios. The length did not decrease noticeably in the nanorod solutions, however widths increased significantly. Varying the heating times and growth solution concentrations result in shapes such as nanocubes and nanorods.

Surface modification of gold nanoparticles has been studied extensively.[64-68] In the use of GNPs for medicinal applications, cytotoxicity is a large concern for *in vivo* functionality. Much focus has been placed on surface ligands and surface exchange is a popular form of modification. Phospholipids and thiols have been exchanged for CTAB surface ligands in many cases and found to reduce cytotoxicity in cell uptake. Ligand exchanges are achieved by centrifuging the GNPs and then redissolving the GNPs in a solution of the alternate ligand. This modification has been found to lower the cytotoxicity allowing for the potential to be used in drug delivery and photothermal therapy.

Photothermal therapy has been employed for phase one clinical trials on dogs with cancer in Ohio. The use of hyperthermia to treat cancer is well-established including radiofrequency ablation, laser-induced photodynamic therapy, and ultrasound ablation.[39,41,69,70] Gold nanorods coated with polyethyleneglycol polymers take advantage of NIR light by producing heat. Surface-Enhanced, Resonant Raman Scattering (SERRS) gives enhanced activity and these SERS-coded NRs are highly stable, are detectable down to extremely low concentrations. In vivo, SERS-coded nanorods are trapped in tumor blood vessels following intravenous injection permitting the heating of the nanorods to high temperatures within the tumor using an externally applied NIR diode

laser. Solid dog tumors have shown significant reduction in tumor size with little side effects using this method.

1.3 – History of gold colloids into the 20th century

Even before the nanoscale was realized. It was discovered that transition metal nanoparticles less than 100 nm in size absorb characteristic colors when they interact with electromagnetic energy. More recently, it has been discovered that the size and shape of nanoparticles is important in the interaction with light. Due to these interactions, GNPs have found uses in drug delivery and plasmonic photothermal therapy.[71,72] However, there are still some problems associated with the stability and biocompatibility of these nanoparticles in solution.

The history of GNPs ranges back to Egypt and China in the 5th century B.C., where it was found that gold salts added to molten glass produced a "ruby red" color in the glass. It was also used as a colorant on ceramics, which gave a red tinge to the materials. Wilhelm Ostwald studied the ancient processes and stated,[2] "This colloidal gold was prepared even in the days of the alchemists by the reduction of gold salts by all kinds of organic substances, including urine." These gold colloids gave characteristic colors of red and purple and eventually led to large-scale use in the ancient societies for decorative purposes.

Colloidal gold became especially popular when it started being used in the staining of glass. The ruby-red color common with colloidal gold gave a vivid stain to glass and was very popular among churches and wealthy families. Of the most famous examples is the Lycurgus Cup. Roman artists crafted it in the 4th century AD.[4] The cup contains a dichroic glass made up of silver and gold nanoparticles. The glass reflects green and transmits red making it "the most spectacular glass of the period, fittingly decorated, which we know to have existed".[5]

Ayurveda in the Hindu culture was the first noted use of gold salts in the medicinal system.[3,73] *Bhasmas* are metallic/mineral preparations combined with herbal extracts from decoctions. They have been widely used to treat a variety of maladies since the 7th century A.D. These treatments are claimed to be biologically produced nanoparticles and many of the desired properties of *Bhasmas* steered away from the metallic characteristics and aimed more towards the plant properties. It is stated, "*Bhasma* must be *Nischandra* (lusterless) before therapeutic application. *Chandratva* (luster) is a character of metal. After proper incineration, luster of metal should not remain." Preparing these potions in this way, the ultimate goal of biocompatibility was inadvertently realized. "*Bhasma* must be *Sukshma* [fine or smooth], so that it can be absorbed by the body easily." Also, "*Slakshna Bhasma* can be absorbed and assimilated in the body without producing any irritation to mucous membrane of gastrointestinal tract."[73] The red colloidal solutions

Figure 1.1 – The Lycurgus Cup showing the dicroic nature of the glass. The 300 ppm silver nanoparticles reflect an opaque green (seen right) while the 50 ppm gold nanoparticles give a translucent red color when light is shined through the glass (seen left).[4,74]

believed to cure everything from a simple cough to tuberculosis, and the specific color of the solutions was important in determining if the solutions were prepared properly and therefore biocompatible.[75]

It wasn't until the 1670's that reproducible color could be produced. German alchemist Johann Kunckel found evidence in experiments performed by Johann Glauber that salts of gold chloride added to glass could give the ruby-red color to glass.[6] Kunckel used this information to produce many works of gold ruby glass. It was found that charging the glass with a solution of gold in aqua regia gives an opaque, grey glass, which upon annealing, produces a ruby-red translucent glass[7] (Figure 2). The science of making red

glass thus became experimentally possible, but it wasn't for another two centuries that the science behind the red color began to be explained.

Figure 1.2 – Examples of ruby-red glassware made by Kunckel's. Included is a covered goblet sold from Kunckel's shop prior to 1691. It is now on display in Hamburg. These are some of the few surviving pieces from the alchemist's works.[6,7]

Michael Faraday was the first to use gold colloids for scientific purposes.[8] In the 19th century, Faraday developed a method of using aqueous gold chloride and phosphorus in CS_2 to synthesize a variety of solutions of GNPs. These nanoparticles ranged from 2 – 100 nm in size and had a variety of colors depending on the pressure applied to them after synthesis. Faraday thus illustrated that the ruby glass was colored so, because of the presence of finely dispersed gold particles. Faraday did note that in these methods, the nanoparticles tended to aggregate when electrolytes and non-polar surfactants were introduced to the solution. His hypothesis that the colors of gold solutions were in fact

colloids was further supported when he carried out reactions to prove that 'Purple of Cassius' could be obtained by adding tin chloride to gold sol. Though colloids had been produced for centuries, it was Faraday's methods that first connected modern science to GNPs.

Other chemists also contributed to the evolution of nanoparticulate chemistry concerning gold. When Zsigmondy began his investigations into the color of ruby glass and formulated a method for preparing colloidal gold (by reducing a dilute, slightly alkaline solution of gold chloride with boiling formaldehyde), he was unaware of Faraday's work. After discovering Faraday's methods, especially reduction using phosphorus, he combined both the synthetic techniques to arrive at a two-step synthesis method, referred to as the seed-mediated method today.[9,10] Zsigmondy first described color differences seen when using polarized light parallel and perpendicular to anisotropic particles.[11] He observed that GNP films on gelatin gave rise to two results: 1) When particles were observed perpendicular to the longer diameter, then the transmitted light is red and diffracted green; 2) On the contrary, if the vibrations are parallel to the longer diameter, then the transmitted light is blue and the diffracted light yellow or brown. These optical properties led to some of the current technologies we use today.

Ostwald's contribution to the study presented many key theoretical principles and in his research he demonstrated the importance of salinity on the growth process of the nanoparticles. He stated, "In order to obtain [colloidal gold] by condensation, I begin with a molecularly or ionically dispersed solution of gold chloride to which sodium

bicarbonate has been added until neutral to litmus. I need now to reduce the gold chloride to metallic gold, but this must be done in such a way that metallic gold remains so highly dispersed as not to exceed colloidal dimensions." He goes on further to explain, "As you know, gold chloride can be reduced by many different kind of substances, especially organic ones. You need but dip your finger into the solution when it becomes stained with bluish violet by the colloid gold produced through the reducing action of the organic substances contained in the skin." In this, Ostwald's remarks demonstrate that the size is key in keeping particles dispersed. From this, we get the term "Ostwald ripening," referring to the equilibria growth of nanoparticles resulting from the surrounding envoironment.

It wasn't until 1951 that the stability of GNPs began to be studied. John Turkevich's work on synthesis of gold colloids using sodium citrate found that GNPs were stable for extremely long periods of time, and also produced GNPs which were fairly mono-disperse by the time period's standard.[76,77] By the end of the 20th century, many new methods were being developed in synthesizing GNPs. In 1973, Gerrit Frens refined work performed by Turkevich in 1951 to give better size control to GNPs using the citrate synthesis. Wilcoxon developed a two-phase method for synthesis of nanoparticles with various polar and non-polar ligands.[78] Brust used hydrophobic thiols in 1993 to synthesize hydrophobic nanoparticles, which are more stabile to aggregation.[79]

More recently, new discoveries in GNP research have led to size and shape control. In short, Michael Natan developed a seed mediated approach to GNP growth based on

patent literature,[80] which led to a more monodisperse synthesis of nanoparticles.[81] Chris Wang's group realized electrochemical methods in synthesizing rod shaped GNPs and Catherine Murphy and Mustafa El-Sayed used the seed-mediated idea as a basis to develop a chemical synthesis of shape controlled GNPs.[52] However, stability of the nanoparticles in solution during a shape controlled synthesis still remains a problem. For the purpose of medicinal use, it is important that these GNPs remain stabile and it has been proposed that natural extracts could be of use in synthesizing anisotropic GNPs.

1.4 – Short history of Soybeans into the 20th Century

At the same time that gold was being used in Egyptian art and jewelry, China was developing another essential resource. Soybeans have been important throughout history, from farming to nutrition, and even to drug delivery.[82,83,84] Soybeans have been a crucial tool used in the rotation of food crops, thus providing a method of fixing nitrogen in the soil. They've also served as a source of protein in feed for livestock. And since the discovery of fermenting, soy has been used as a staple in a multitude of different cuisines such as Japanese (miso, edamame), Chinese (soy sauce) and has received huge accolades in the vegetarian diet (tofu, tempeh, soy milk, soy cheese, etc.). Soybeans have even been used to make milk substitutes for the lactose intolerant.

Soybeans have been around since ancient times. The first records of soybeans were written in 2853 B.C. when the Chinese Emperor Shennong proclaimed soy a sacred plant.[85] It was slowly introduced to other Asian cultures such as Korea and Japan over the

next millennium and became a key ingredient in the local cuisine. Preserved soybeans have been found in Korea and date back to 1000 B.C. The beans were used to produce tofu and soy milk and used on a large scale by the orient. These legumes were consumed in the typical diet of the Asian population, however, they did not make their way to other subcontinents until the 18th century.

Around the beginning of the 1st century, fermentation of the soybean was discovered and allowed for removal of phytoestrogens found in raw soybeans.[85] This lead to the introduction of soy sauce and miso into average households and a new revolution of food was introduced to the world. Due to its popularity and the development of trade routes, the soybean soon spread to the rest of the Asian continent. However, the soybean was not introduced to Europe until 1739 when the first plants were cultivated in France. It was reported that Benjamin Franklin sent seeds of the bean to the Pennsylvania colonies of the New World to be planted by his botanist friend, John Bartram, in 1770.

Soybeans have become a huge influence in all nations for food stocks and have been attributed to longevity of life and health.[86] The Okinawa Centenarian Study states, "Okinawan elders eat an average of two servings of flavonoid-rich soy products per day." They also report, "This enormously reduced cancer risk arises in part, the study's authors say, from the Okinawans large consumption of isoflavones from soy. This is an important finding." "Okinawans are at extremely low risk for hormone–dependent cancers, including cancers of the breast, prostate, ovaries, and colon. Compared to North Americans, they have a staggering 80 percent less breast cancer and prostate cancer, and

less than half the ovarian cancer and colon cancer."

In modern times, the soybean has remained a key food staple in the world diet, however, it has also evolved into a scientific field. Many books and journals have been introduced solely dedicated to soybeans and the health and chemical characteristics of the legume. The chemical content of the soybean makes for a wide variety of topics to be discussed. The phytoestrogens, isoflavins and Omega-3 fatty acids have made it a hot topic in medical journals and the phospholipids it contains are a huge source of scientific study due to their ability to assemble into multilayered isoforms.[87-92] The liposomal nature of the phospholipids allows scientists to obtain a cheap source mimicking lipid bilayers, the backbone of all biological cells and therefore, provide a potential biocompatible element.

More recently, soybean proteins and phospholipids have been proposed in drug delivery systems.[93,94,95] Use of lipid emulsions and hydrolyzed polymeric lipids have shown great promise in drug delivery. In every case, the delivery systems were tested for cytotoxicity and biocompatibility and found that in many cases, the natural product was completely safe for use in human physiology.[93-96] Even more research has been performed to test the biocompatibility of these substances when encapsulating anisotropic GNPs. The optical properties of anisoptropic transition metal nanoparticles, especially gold and silver, has become of considerable interest when being used in biosensors and therapeutics, and for the use in biological systems, the gold and silver nanoparticles must be biologically adaptable.

Theory of Optical Properties of Gold Nanoparticles

2.1 – Physical properties of Gold Nanoparticles

The study of nanotechnology is highly dependent on the ability to create and manipulate materials in the range of 1 – 100 nm.[97-109] This will lead to smaller, faster, cheaper materials for data storage, energy manipulation and medical devices in which the devices fabricated will approach the size of individual molecules. The nanoscale is put into context in Figure 2.1, which shows the size change from a soccer ball down to a buckyball. In downsizing materials to the nanoscale, it has been discovered that the nanoscale properties of materials are sometimes extremely different from their bulk counterparts, giving interesting properties.

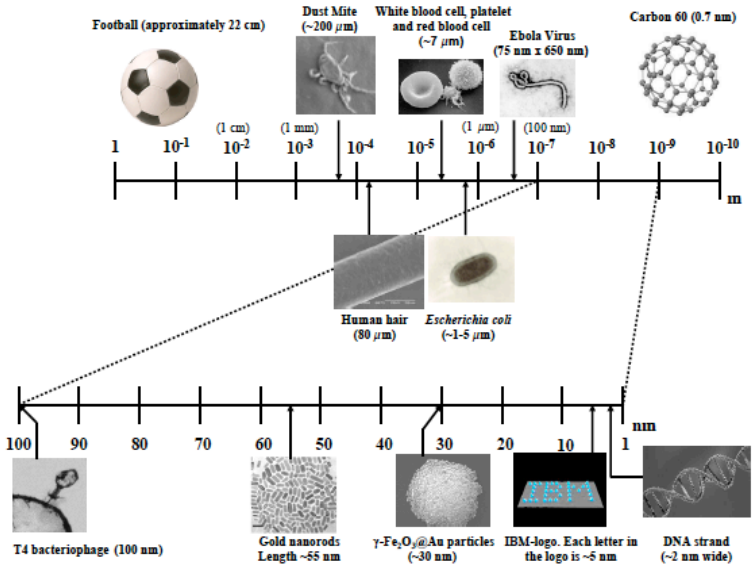

Figure 2.1 – Contextual visual scaling down from the size of a soccer ball, through biological oligomers to nanomaterials such as a buckyball.[110]

Two principal driving forces behind the differing properties are an increase in the surface area of the material and the size-dependent properties, which dominate in the nanoscale. This affects the chemical reactivity, electrical, optical and thermal properties of the material. This can lead to promising uses for the nanomaterials such as catalysis, photovoltaic and medicinal uses. Gold for example is being studied for medicinal purposes due to its non-toxic nature and its change in reactivity from bulk to the highly reactive nanoscale.[16,17,18]

2.2 – Gold Chemistry

Gold has been thoroughly studied by scientists in order to understand the inert nature of the metal. It is important to understand the redox potentials of gold in order to explain its nobility. In order for any reaction to occur with gold, it first must be oxidized,

$$Au \rightarrow Au^{+}_{aq} + e^{-} \qquad 2.1$$

The reduction potential can be explained using the Nernst equation:

$$E = E^{\circ} - 2.303\frac{RT}{F}\log_{10}\frac{[Au]}{[Au^{+}]}$$

where R is the gas constant, F the Faraday constant, T the absolute temperature and E° the standard electrode potential for the reaction (~ 1.7 V). Solving this gives

$$E = 1.7 + 0.059 \log_{10} [Au^{+}]$$

Gold has two oxidation states, the +1 and the +3 so solving for the +3 state gives

$$Au \rightarrow Au^{3+}_{aq} + 3e^- \qquad 2.2$$

$$E = 1.50 + 0.0197 \log_{10} [Au^{3+}]$$

Gold can also react with its environment.

$$Au + 3H_2O \leftrightharpoons Au(OH)_3 + 3H^+ + 3e^-$$

$$E = 1.46 - 0.059 \text{ pH}$$

Further reaction gives

$$Au(OH)_3 \leftrightharpoons AuO_2 + H_2O + H^+ + e^-$$

$$E = 2.63 - 0.059 \text{ pH}$$

This, of course, can only happen if strong oxidants are present. To discuss the equilibrium between auric hydroxide and auric ions,[111] a constant concentration is used. At $[Au^{3+}] = 10^{-4}$ M

$$Au^{3+} + 3H_2O \leftrightharpoons Au(OH)_3 + 3H^+$$

$$\text{pH} = -\frac{1}{3}\log_{10}[Au^{3+}] - 0.693$$

Water's stability also limits the electrochemistry driven by a voltage to oxidize to oxygen or reduce to hydrogen. This is shown by

$$2H_2O \leftrightharpoons O_2 + 4H^+ + 4e^-$$

$$E = 1.229 - 0.059 \text{ pH}$$

or

$$2H_2O + 2e^- \leftrightharpoons 2OH^- + H_2$$

$$E = 0.0017 - 0.059 \text{ pH}$$

It can be concluded that gold cannot be oxidized in dissolved oxygen with strong acids or

alkalis. Gold is the only element with this property giving more credit to its nobility.

Gold dissolves in solution containing gold-specific ligands and an oxidizing agent, however these alone are not adequate. For example, gold does not dissolve in HCl or HNO_3 alone, but in aqua regia, $HAuCl_4$ is formed. Similarly, CN^- needs oxygen from air or an oxidizing liquid to dissolve gold metal.[112] A generalization is written as

$$Au + 2CN^- \rightarrow [AuCN_2]^+ + e^-$$

which is further oxidized to Au^{III} by

$$[AuCN_2]^+ + 2CN^- \rightarrow [AuCN_4]^{3+} + 2e^-$$

Returning to the standard potentials, it is seen that good ligands with high *K* values give a low E° value according to the Nernst equation. It is seen that the ionic gold atoms cannot exist in solution free, but form complexes with the ligands present. If water is the only available ligand, it can form the aqua ions form, $Au(H_2O)_2^+$ and $Au(H_2O)_4^{3+}$. Substituting chloride in gives

$$Au(H_2O)_2^+ + 2Cl^- \leftrightharpoons [AuCl_2]^- + 2H_2O$$

$$Au(H_2O)_4^{3+} + 4Cl^- \leftrightharpoons [AuCl_4]^- + 4H_2O$$

2.3 – Gold^{III} complexes

The complex $HAuCl_4$ was shown to be made using aqua regia. Substituting HBr for HCl similarly gives $HAuBr_4$. Evaporation of the solution, followed by washing with the respective halogenated acids generates hydrated forms of the molecule (i.e. – $HAuBr_4 \cdot xH_2O$). The important aspect of this is that the gold complexes of these compunds have a low-spin $5d^8$ electron configuration, giving a four coordinate square planar stereocenter.

This allows reaction with the gold center more easily. This can also be seen in other group 10 and group 11 metals such as platinum.

This leads to the interesting optical properties. Figure 2.2 shows the molecular orbital diagram for a square planar Au^{III} complex[113]

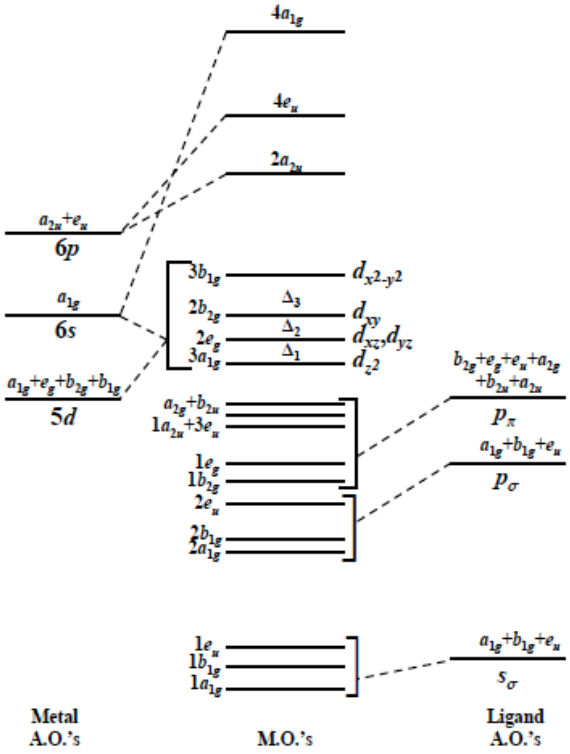

Figure 2.2 – Molecular Orbital diagram for square-planar Au^{III} complex[114]

Au^{III} has a d^8 electronic configuration in which all of the 5*d* orbitals are double occupied except the $d_{x^2-y^2}$. The energy differences between the occupied *d* orbitals give weak ligand to field transitions at low energy. This can be seen in Figure 2.3 showing the absorption spectra of $HAuCl_4$ and $HAuBr_4$ (both at 10^{-4} M in methanol). The difference in intensity shows that the extinction coefficients are not isolated to the metal *d* shell, but

correspond to the ligand to metal charge transition.[115] This leads to an increased absorption at a longer wavelength for the $HAuBr_4$. The shifted absorbance is due to a lower ionization potential over the chloro-derivative as it gets easier to oxidize the halide.

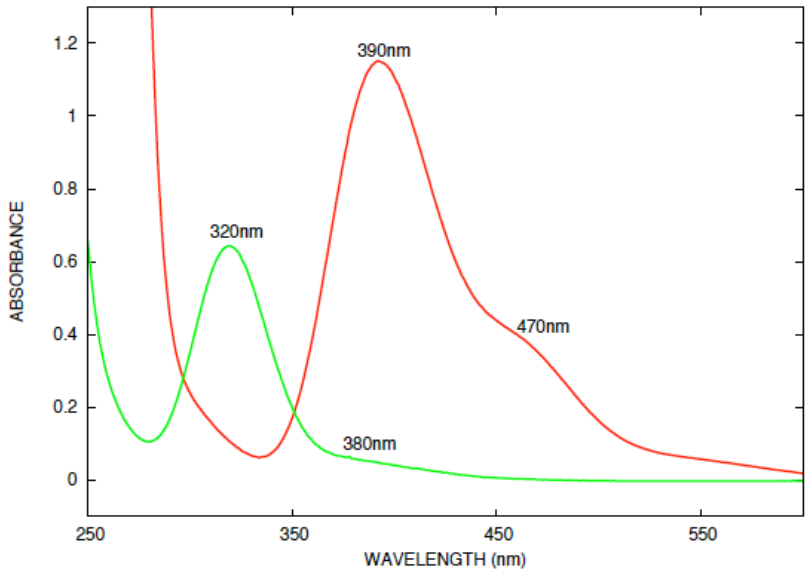

Figure 2.3 – Absorption spectra of $HAuCl_4$ (green trace) and $HAuBr_4$ (red trace). Both have concentrations of 10^{-5} M and are dissolved in methanol.[116]

2.4 – Colloids

Metal colloids are an example of a lyophobic colloid (as opposed as lyophilic colloids like proteins). These colloids are thermodynamically unstable unless they are either kinetically stabilized by a charge (electrostatic stabilization) or separated by adsorbed ligands preventing their approach to each other (steric stabilization). This prevents aggregation of the colloids leading to coagulation of the particles out of solution. It is the steric stabilization that is the most common form of stabilization when using metal

nanoparticles.

Addition of a soluble lyophilic material, such as amphipathic surfactants, leads to repulsion of the particles.[117] The lyophilic materials usually contain two components, one that adsorbs to the surface of the metal, while the other is soluble in the dispersion medium. In order to describe the total potential energy (V_T) of interaction is calculated:

$$V_T = V_R + V_A + V_S$$

in which V_R is the repulsion potential energy, V_A is the attraction potential and V_S is a structural term. The Van der Waals attractions between particles is relatively small (Figure 2.4) where the potential barrier for the dispersion is minimal. The less important

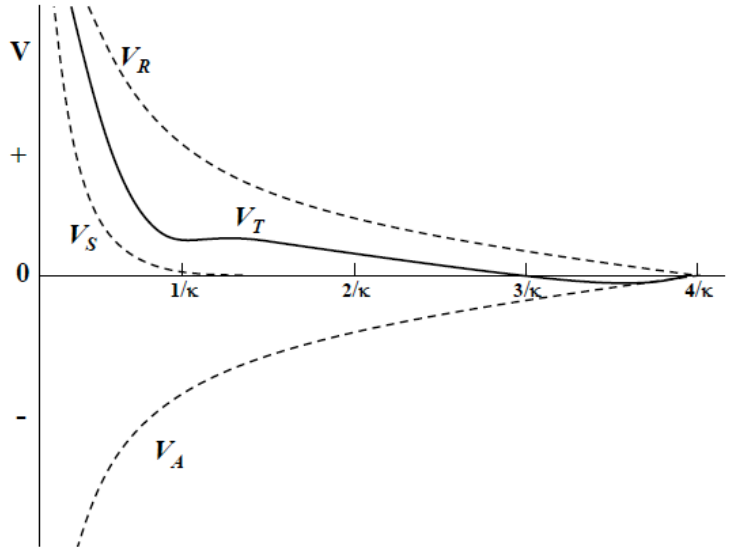

Figure 2.4 – Potential diagram for sterically stabilized particles ($V_T = V_R + V_A + V_S$)[114]

contribution of the Van der Waals attraction in inducing aggregation of sterically stabilized dispersions is in sharp contrast with its role in causing coagulation in

electrostatically stabilized dispersions. The steric stabilization thus depends on the adsorbed ligands and when two of the protected particles approach one another, thermodynamically the ligating material experiences a loss of entropy and a gain in free energy. This results in a repulsion of the particles.[118] This protects colloids from aggregation by electrolytes in both aqueous and non-aqueous media.

2.5 – Optical properties of metal nanoparticles

As the synthesis of GNPs developed in the 20th century, physicists began working on calculations to explain the optical properties of colloidal gold. Mie founded an incredible breakthrough in this area.[119] Motivated to explain the color, he calculated the theoretical absorption and scattering patterns given off by metal particles. His paper included the calculation of absorption spectrum for gold sols in water, as well as absorption and scattering spectra as a function of particle size for spherical gold particles.

Metal colloids, such as silver and gold, with $r \ll \lambda$ respond to incident electromagnetic waves as seen in Figure 2.5. This scheme depicts the influence of the external field on the electrons on the surface of the particles. The electrons are displaced from the positive charges in the metal and thus provide Mie resonances or surface plasmon resonances.[120] This term comes from the effect producing the restoring force being the surface polarization.

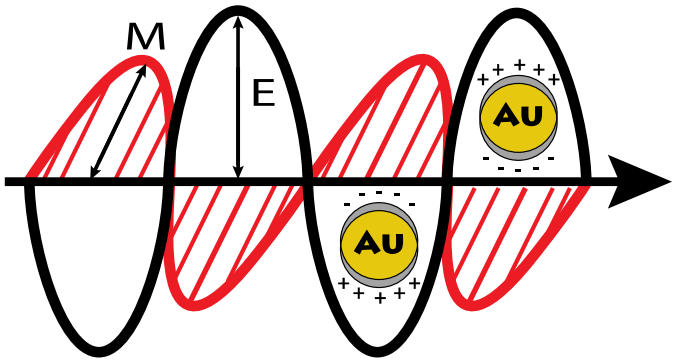

Figure 2.5 – Interaction of spherical particles with external electromagnetic field

The colloid's color can be described using the dielectric function, $\varepsilon(\omega)$. In colloids with a diameter larger than 10 nm, the function has a value of the bulk metal. When the colloids have diameters smaller than 10 nm, the dielectric functions vary as a function of particle size.

The Lorentz-Drude-Sommerfeld Model helps to explain the optical properties by treating the ions and electrons as simple harmonic oscillators.[121] Using this model, the understanding of collective oscillations of free electrons is elucidated. In this theory, the electrons are assigned an m_e and a velocity v giving an electric field of

$$E = E_0 \exp(-i\omega t) \qquad 2.3$$

At frequency ω, the electron in the metal is accelerated and collides with the lattice, other electrons and impurities present in the material at a rate proportional to v. When collisions occur, v is reduced to 0 and the average velocity of a single electron can be

calculated to $eE\tau/m_e$ where τ is the time between collisions. If we apply this to a collection of electrons, the polarization P in an isotropic media connects the dielectric function defined by

$$P = \chi\varepsilon_0 E = \varepsilon_0(\varepsilon\text{-}1)E \tag{2.4}$$

where χ is the electric susceptibility. If we further express the dielectric function in terms of the electric susceptibility, we get

$$\varepsilon(\omega) = 1 - \frac{Ne^2/m_e\varepsilon_0}{\omega^2 + i\omega_d\omega} = 1 - \frac{\omega_p^2}{\omega^2 + i\omega_d\omega} \tag{2.5}$$

where $\varepsilon(\omega) = \varepsilon_1(\omega) + i\varepsilon_2(\omega)$ and is the dielectric function for free electrons per unit volume and $\omega_p = (N\hat{e}^2/m_e\varepsilon_0)^{1/2}$ is the Drude plasma frequency in terms of N (concentration of free electrons in metal).[122] The dielectric function can then be defined as

$$\varepsilon_1(\omega) = 1 - \frac{\omega_p^2}{\omega^2 + \omega_d^2}$$
$$\varepsilon_2(\omega) = \frac{\omega_p^2\omega_d}{\omega(\omega^2 + \omega_d^2)} \tag{2.6}$$

This is the Drude model for optical properties for a free-electron metal and can be used to describe the concentration of electrons on the surface as seen in Figure 2.5.

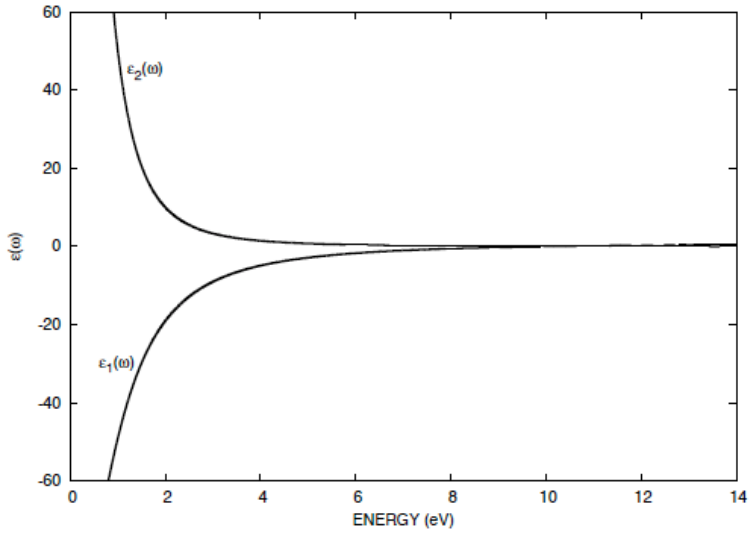

Figure 2.6 – The real and imaginary parts of $\varepsilon(\omega)$ of a Drude model as a function of frequency (ω) in eV. ω_p = 10 eV and ω_d = 1 eV.[114]

Figure 2.6 shows that when the applied field shifts the oscillating electrons out of phase, $\varepsilon_1(\omega)$ is negative over a wide range. Also, $\varepsilon_1(\omega)$ is negative in the frequency below the the bulk plasma frequency (ω_p) of the metal due to the polarization field being larger and opposite in sign to the applied field.

This model explains the optical response to a collection of free electrons without a restoring force. Since metal nuceii are shielded by neighboring conduction electrons, a restoring force is not available except when a small dipole is created by an incident light wave. This sets up a surface polarization allowing the free electrons to have a restoring force and oscillate. Since the displacement of electrons is not in phase with the applied field, the displacement can be written as $Ae^{j\phi}(eE/m_e)$ with amplitude A and phase angle ϕ.[122] These are defined as

$$A = \frac{1}{\sqrt{[(\omega_0^2 - \omega^2)^2 + \omega_d^2 \omega^2]}}$$
$$\phi = \tan^{-1} \frac{\omega_d \omega}{\omega_0^2 - \omega^2} \qquad 2.7$$

The amplitude can be plotted as a function of frequency (in eV) as seen in Figure 2.7

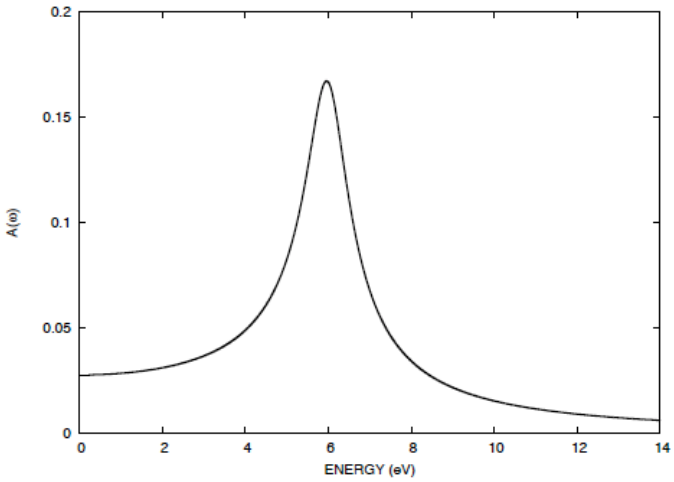

Figure 2.7 – Plot of A of a one-oscillator (Lorentz) model. $\omega_0 = 6$ eV and $\omega_d = 1$ eV.[105]

The maximum is seen where $\omega \cong \omega_0$ and its height full-width-half-max is inversely proportional to ω_d.

When solving for a multi-electron system, the harmonic oscillator equation is expanded to

$$\varepsilon(\omega) = 1 + \frac{N\hat{e}/m_e\varepsilon_0}{\omega_0^2 - \omega^2 - i\omega_d\omega} = 1 + \frac{\omega}{\omega_0^2 - \omega^2 - i\omega_d\omega}$$
$$= 1 + \frac{\omega_p^2(\omega_0^2 - \omega^2)}{(\omega_0^2 - \omega^2)^2 + \omega_d^2\omega^2} + i\frac{\omega_p^2\omega_d\omega}{(\omega_0^2 - \omega^2)^2 + \omega_d^2\omega^2} \qquad 2.8$$

in which N is the free electron concentration. The real and imaginary dielectric function are then respectively extrapolated as

$$\varepsilon_1(\omega) = 1 + \chi' = 1 + \frac{\omega_p^2(\omega_0^2 - \omega^2)}{(\omega_0^2 - \omega^2) + \omega_d^2\omega^2}$$
$$\varepsilon_2(\omega) = \chi'' = \frac{\omega_p^2\omega_d\omega}{(\omega_0^2 - \omega^2)^2 + \omega_d^2\omega^2} \qquad 2.9$$

This leads to the Lorenz model for a concentration of electrons in a metal having a restoring force. The optical amplitude can be plotted versus amplitude to reveal

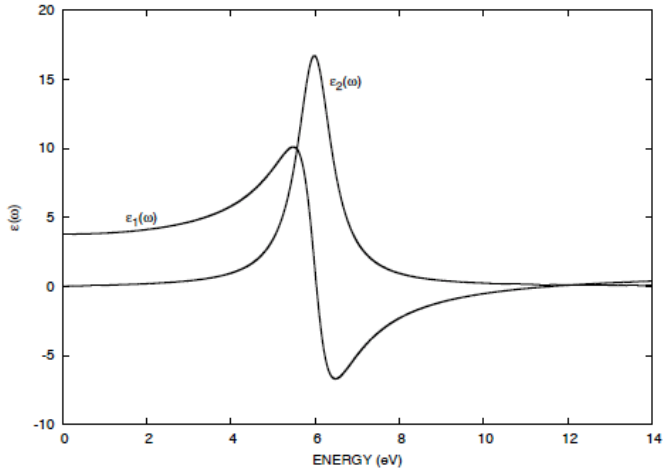

Figure 2.8 - Plot of A of a Lorentz model with the real and imaginary parts of the dielectric function of a harmonic oscillator. ω_p = 10 eV , ω_0 = 6 eV and ω_d = 1 eV[105]

In Figure 2.8, it is seen that $\varepsilon_1(\omega)$ is negative at ω_0. The figure helps explain of the effect of absorption of the surface plasmon resonances for metal nanoparticles as compared the the bulk metal.

2.6 – Nanoparticle Absorption of Light

Loss of intensity of an incident light when interacting with nanoparticles is related to the nanoparticle's absorption and scattering cross sections. The intensity loss by absorption and elastic scattering result in a total extinction cross section

$$\sigma_{ext} = \sigma_{abs} + \sigma_{sca} \tag{2.10}$$

The Beer-Lambert law can be used to calculate the intensity of transmitted incident light, *I(x)* in relation to the extinction cross section using the formula

$$I(x) = I_0 e^{-N\sigma_{ext}x} \tag{2.11}$$

where I_0 is the intensity of the attenuation of a parallel beam of incident light and x is the path length in cm. This can be related to absorbance, A, by taking the log[123]

$$A = \log_{10}\left(\frac{I_0}{I(x)}\right) = \frac{N\sigma_{ext}x}{2.303} \tag{2.12}$$

Mie theory can be used to expand the fields into partial waves of different spherical symmetries.[120] The dielectric function ε_m, the extinction cross section of a medium, with embedded nanoparticles is used in the expansion. The Mie formula can be simplified to

$$\sigma_{ext}(\omega) = 9\frac{\omega}{c}\varepsilon_m^{3/2}V_0\frac{\varepsilon_2(\omega)}{[\varepsilon_1(\omega)+2\varepsilon_m]^2+\varepsilon_2^2(\omega)} \tag{2.13}$$

with $V_0 = 4/3\pi r^3$ the particle volume and $\varepsilon(\omega)$ the dielectric function of the particle. The real part of the dielectric function is defined as

$$\varepsilon_1(\omega) = \varepsilon^{\infty} - \frac{\omega_p^2}{\omega^2+\omega_d^2} \tag{2.14}$$

with ε^{∞} the high frequency dielectric constant. We can then use this to plot an absorption model of spherical nanoparticles (Figure 2.9). The damping parameter ω_d is related to the

mean free path of the conduction electrons, R_{bulk} and and the velocity of the electrons at the Fermi energy v_f[124]

$$\omega_d = \frac{v_f}{R_{bulk}} \qquad 2.15$$

So as particle size decreases, the damping parameter increases causing the band to broaden and the intensity to decrease.

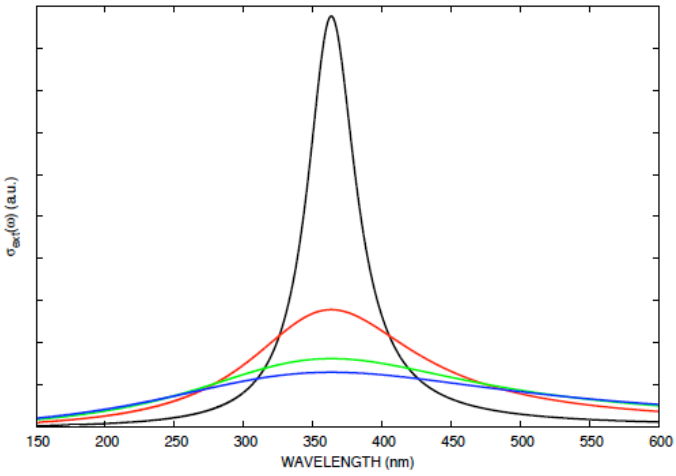

Figure 2.9 – Calculated absorption band for surface plasmon resonance of silver colloids. Mie dipole approximations show the effect of the damping parameter ω_d. As the ω_d increases, the intensity drops. The damping frequencies in eV are 0.4 (black), 1.4 (red), 2.4 (green) and 3.0 (blue).[124]

2.7 – Effect of nanoparticle size on plasmon band

There is no size dependence in the dipole approximation (Equation 2.13) except for the intensity change from nanoparticle's volume V_0 with radius r. The position of the plasmon absorption max (λ_{max}) has been seen to have a red or blue shift depending on size.[120,125] El Sayed's group studied the size of colloidal GNPs between 9 and 99 nm and found that the plasmon band red-shifts with increasing diameter as seen in Figure 2.10.

The figure shows absorptions from silver nanoparticles ranging from 10 nm to 100 nm revealing a red-shift with increasing size.

Mie theory does not account for size dependence and the dielectric function must be altered to account for the diameter of the nanoparticles $[[\varepsilon = \varepsilon(\omega, r)]$. This size dependence is only seen for nanoparticles with a diameter smaller than the mean free path of the conduction electrons.[126] This results in a size-dependent absorption cross section in the dipole approximation, or commonly known as an intrinsic size effect.[120] The average electron collision time, τ (relaxation time), is the average of the τ_I which is an effect from collisions with phonons, lattice defects and impurities.[125,126]

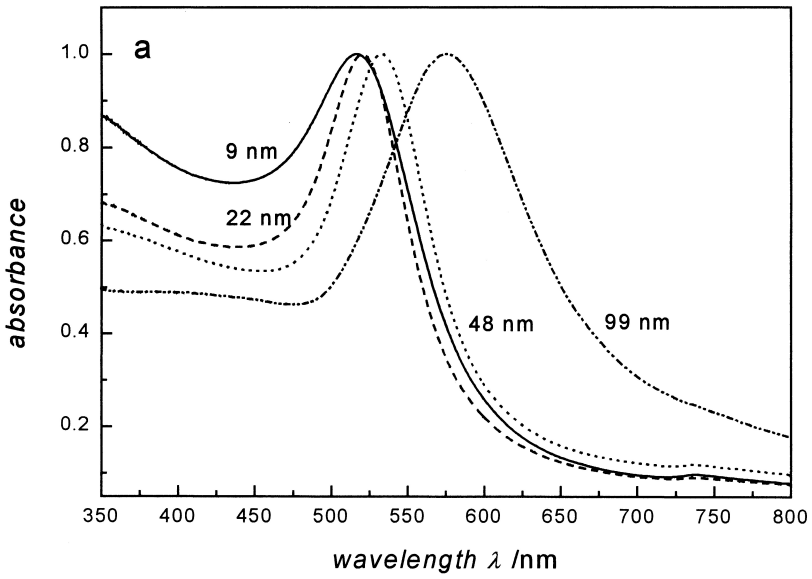

Figure 2.10 – Absorption spectra of spherical gold nanoparticles of varying sizes. The spectra are normalized at their plasmon absorption maxima. The corresponding shifts are 517 nm for a 9 nm particle, 521 nm for a 22 nm particle, 533 nm for a 48 nm particle and 575 nm for a 99 nm particle.[125]

The damping constant γ is related to the collision time by

$$\gamma = \tau^{-1} = \sum_i (\tau_i)^{-1} \qquad 2.16$$

The surface of small particles acts as another collision process due to the comparable size of the particles to the mean free path of electrons, which in very small particles reduces the effective mean free path. This is dominated by the collision of conduction electrons with the particle's surface, therefore the particle radius *r* requires the damping constant to be calculated as[125,126]

$$\gamma(r) = \gamma_0 + \frac{A \cdot v_f}{r} \qquad 2.17$$

where γ_0 is the bulk damping constant seen in equation 2.16, v_f is the velocity of the conduction electrons at the Fermi energy and *A* is the specific scattering processes.[125]

For larger nanoparticles ($r > 15$ nm), the extinction cross section depends on higher-order multipole modes within the Mie equation. The extinction spectrum is consequently dominated by dipole absorption as well as quadrupole and octopole absorption and scattering processes.[125] The superposition of the multipole oscillations peaking at different energies contributes to the total plasmon band absorption. Retardation effects lead to the broadening of the plasmon band though the increase in FWHM can also be caused by the interaction the dipole and the higher-order oscillatory motions of the electrons.[125]

This leads to an *extrinsic size effect,* which affects the plasmon resonance when the complex dielectric function of the bulk material is used in the Mie equation and size is no longer a factor.

2.8 – Ansiotropic Nanoparticles and their Light Absorption

Mie's theory is only applicable to spherical particles. When Mie compared his theoretical plots to that of the experimental results of his research, Mie observed a deviation in the spectra in certain cases.[119] Mie believed the behavior was from ellipsoidal particles. This has been explained for rod-shaped nanoparticles, also known as nanorods. For nanorods, the orientation of the particle axis dictates the plasmon oscillation of electrons with respect to the oscillating electric field of incident light. The result is two absorption bands, one being for the transverse resonance and the other for the longitudinal resonance.[127] Figure 2.11 shows the electron cloud modes interacting with incident light in both modes.

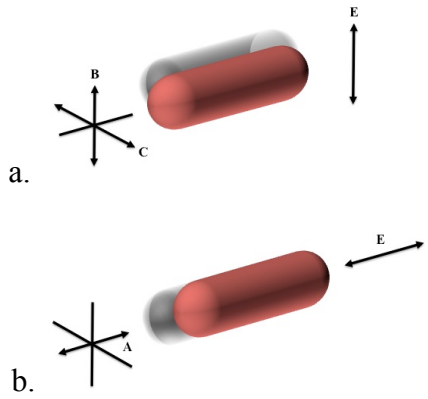

Figure 2.11 – Schematic of two oscillating modes of nanorods. These modes give a transverse oscillation (figure a) and a longitudinal oscillation.

The properties of the metal nanorods can be explained using Gans theory. Gans extended

the Mie theory to consider spheroid particles.[128] He found that smaller aspherical particles allowed for plasmon bands at longer wavelengths than spherical particles of comparable size. It should be noted that in sub-nm sized particles, quantum mechanical methods don't allow for continuous density of states. Therefore, very small metal nanoclusters do not display the plasmon resonances seen for larger free-electron metal nanoparticles.[129] According to Gans theory, the extinction coefficient (κ) for N nanoparticles with volume V_0 can be expressed in the dipole approximation as[130,131]

$$\kappa_{\text{ext}} = \frac{2\pi N V_0 \varepsilon_{\text{m}}^{3/2}}{3\lambda} \sum_j \frac{\left(\frac{1}{P_j^2}\right)\varepsilon_2}{\left[\varepsilon_1 + \left(\frac{1-P_j}{P_j}\right)\varepsilon_{\text{m}}\right]^2 + \varepsilon_2} \tag{2.18}$$

in which P_j are the depolarization factors used to calculate absorption of nanorods for the three axes A, B, and C seen in Figure 2.11. The geometrical factors P_j for the nanorods along the respective axes are

$$P_A = \frac{1-e^2}{e^2}\left[\frac{1}{2e}\ln\left(\frac{1+e}{1-e}\right) - 1\right] \tag{2.19}$$

$$P_B = P_C = \frac{1-P_A}{2} \tag{2.20}$$

with

$$e = \sqrt{1-\left(\frac{d}{L}\right)^2} = \sqrt{1-\frac{1}{R^2}} \tag{2.21}$$

where R is the aspect ratio defined by L/d.[130,131] El-Sayed's group calculated the absorption spectra of gold nanorods using equation 2.18 for a series of aspect ratios with

measured dielectric functions. This is illustrated in Figure 2.12 where El-Sayed's group modeled several sizes of nanorods with aspect ratios from 2.6 to 3.6. Using a medium dielectric constant of 4, it was shown that longitudinal plasmon band red-shifts 150 nm as the aspect ratio increases. It is also shown that the red-shift in absorption maxima of the longitudinal band follows a linear trend.

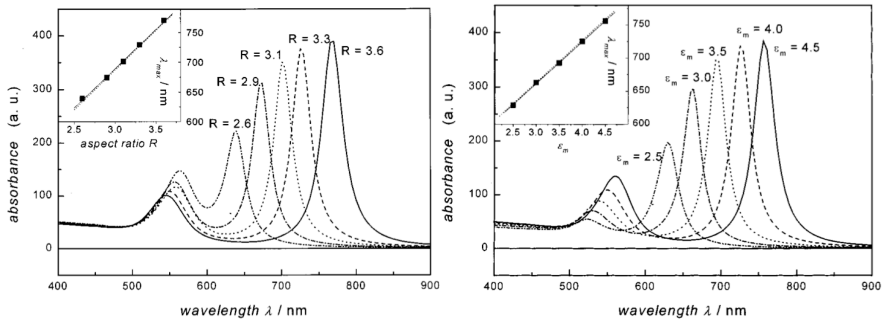

Figure 2.12 – Absorpton calculations of nanorods with increasing aspect ratio and increasing dielectric constants respectively. Both show linear shifts in absorption maxima for the longitudinal plasmon band (inserts).[130]

An equation was then extracted to approximate the l_{max} with aspect ratio R and dielectric constant e_m as[130]

$$\lambda_{max} = (33.34R - 46.31)\varepsilon_m + 472.31 \qquad 2.22$$

We can see that both the aspect ratio and the dielectric constant give a linear response to the incident light. For example, in Figure 2.12, a graph of the λ_{max} versus various dielectric constants at a constant aspect ratio of 3.3 reveals a linear regression.

Synthesis of Gold Nanoparticles in Soy Lecithin

3.1 – CTAB standard versus Soy Lecithin

Introduction

As previously discussed, the electronic and optical properties of nanoparticles are determined by both their size and shape.[97-109] Chemically influencing the shape of GNPs has been studied by many methods. A seeded method using cetyltrimethylammonium bromide (CTAB) is the most popular method for synthesizing anisotropic GNPs.[52,130-138,146] Small gold seed particles between 4 and 5 nm are synthesized using a strong reductant. These seeds allow for a nucleation site for larger gold nanoparticles to grow. CTAB can then be used as a directing agent, allowing for growth in one or two dimensions depending on the growth environment.[44,56,59,62,132] Its seen that when using CTAB with $HAuCl_4$ as a growth solution, rod shaped nanoparticles could be synthesized with great efficiency.[132] However, if the growth solution is altered by removing seed and a competing halide salt is added, such as KI, prismatic nanoparticles are produced. A difference in seed morphology also produced different shapes of GNPs. Sionnest's group showed that multiply twinned seeds added to a growth solution in the presence of $AgNO_3$ (catalyst) gave a bipyramidal shaped GNP while Pérez-Juste *et. al.* found that using multiply-twinned seeds with no catalyst produced nanorods containing penta-twinned facets running the length of the nanorods.[133]

Although CTAB is versatile as a shaping agent in GNP growth, the biocompatibility of GNPs grown in CTAB have not shown great promise.[134] Many methods of manipulation

have been employed to correct this. One popular method is ligand exchange using natural extract.[65,135] Soybeans have been used as a stabilizing agent against nanoparticle aggregation in many instances.[136,137,138,139]

Soy lecithin has been of considerable interest due to the presence of phospholipids, the main building block of cell membranes.[140-145] One of the more popular components present in soybean lecithin for ligand exchange is phosphatidylcholine (PC). PC consists of a phosphocholine head-group attached to a glycerol linker. Each of the two remaining oxy groups on the glycerol contains fatty acids. These fatty acids are composed of a long carbon chain, which are either saturated or contain any number of double bonds (Figure 3.1). However, PC is not the only phosolipid component present in soybeans. Many other components are present such as phosphatidylethanolamine (PE), lyso-phospholipids in which one of the fatty acid tails are missing, and phosphatidic acid (PA), which lacks a carbonyl chain off the phosphate head group.

PC has often been used for multiple reasons.[146-152] Its similar structure to CTAB makes it a possible shape-directing agent. Its makeup in nature gives it viability for biocompatibility. And its ability to organize into micelles makes it ideal for prevention of aggregation of GNPs. The lamellar nature of lecithin in aqueous media allows for possible growth of nanomaterials in the aqueous cavities of the resulting liposomes. Micelles form when the hydrophobic ends of the phospholipids flock together in the interior of the sphere while the polar head-groups are exposed to the water. These nanoreactors can restrict the size of the particle according to the size of the interior of the

micelle. These droplets are randomly displaced and subjected to Brownian motion, exchanging their water content and reforming into two different micelles.[139] This allows for reformation of the micelles giving rise to different products in the nano-scale. This makes the micelles ideal for materials synthesis.

It has been shown that the bromide ion in CTAB performs an ionic exchange with chloride ions in the gold compounds. Thus an alternate crystal facet is formed when stacking of the gold atoms occurs.[150] This in turn causes stacking in a pentafold twinned crystal facet along the [110] direction. The sections are separated by (111) planes containing {100} side facets as seen in HRTEM.[151] This anion exchange can be tracked using UV-Vis spectroscopy.[116]

Using soy lecithin, we set out to mimic the CTAB synthesis and make gold nanorods. What we found was that the plethora of components cause different reactions to take place and, although PC is a common ligand exchange agent, PC is not ideal for the synthesis of gold nanorods. We found that PA was a better reagent for anisotropic growth, and though it produces prismatic shapes, the resulting optical properties followed those of gold nanorods.

3.2 – Experimental

L-α-Phosphatidylcholine Type IV-S ≥ 30% TLC (PC_{30}), cetyltrimethylammonium bromide (CTAB), potassium cyanide and Agarose Type II Medium EEO, and L-ascorbic acid were purchased from Aldrich. Hydrogen tetrachloroaurate (III) hydrate and hydrogen tetrabromoaurate (III) hydrate were purchased from Strem Chemicals Inc. Potassium bromide was purchased from Acros. Sodium borohydride (98%) was purchased from J.T. Baker. L-α-Phosphatidylcholine (Soy-95%) and L-α-Phosphatidic Acid (Egg, Chicken-Monosodium Salt) were purchased from Avanti Polar Lipids. Centrifugation was performed on a Sorvall RC-6 equipped with a SS-34 rotor. Samples were run at 3000 rpm (1068 x g) for 20 minutes. Milli-Q H_2O was used at 18.1 mΩ resistance.

Preparation of $HAuBr_4$ with CTAB

A 10 mM solution of $HAuCl_4$ was prepared by dissolving solid $HAuCl_4$ (450 mg, 0.132 mmol) in milliQ water (13.2 mL). Diluted solutions were further prepared using milliQ water (1.25 mM, 0.625 mM, 0.313 mM and 0.156 mM). A 100 mM solution of cetyltrimethylammonium bromide was prepared by adding CTAB (716.0 mg, 1.96 mmol) to milliQ water (19.6 mL). This was added to the gold solutions containing 0.313 mM and 0.156 mM $HAuCl_4$ and UV-Vis spectra were taken both with and without added CTAB (1.0 M).

Preparation of $HAuBr_4$ with KBr

A solution of potassium bromide was prepared by adding KBr (119.0 mg, 2.02 mmol) to milliQ water (1.2 mL). $HAuCl_4$ solution (10 mM) was diluted to 0.313 mM. Several solutions were prepared and to each sample of $HAuCl_4$ was added KBr_{aq} in varying amounts [0.5x (Br^- to Cl^-) - 6.0x]. UV-Vis spectra were taken of each solution. All dilutions were made using milliQ water.

Preparation of CTAB gold seed

CTAB seed was prepared fresh prior to each experiment. Briefly, CTAB (100 mM, 5 mL) was stirred vigorously at 30°C and $HAuCl_4 \cdot xH_2O$ (10 mM, 125 μL) was added followed by immediate addition of $NaBH_{4aq}$ (10 mM, 300 μL). The resulting brown seed solution was allowed to react 45 min to one hour prior to use.

Preparation of CTAB growth solution

To CTAB solution (10 mL, 100 mM) at 30°C was added $HAuCl_4$ (250 μL, 10 mM), $AgNO_3$ (400 μL, 10 mM) and HCl (100 μL, 1 M). While stirring vigorously, ascorbic acid (80 μL, 100 mM) was added and when color disappeared completely, CTAB seed (25 μL) was added and allowed to react 18 h prior to analysis.

Preparation of PC_{30} liposomes

PC_{30} stock solution was prepared by dissolving PC_{30} (200 mg, 0.080 mmol) in minimal cyclohexane, which was immediately dried by rotary evaporation to give a thin film. H_2O

(20 mL) was then added to the vial which was shaken 30 seconds. The cloudy solution was then sonicated for 15-20 min, upon which the solution became translucent.

Preparation of PA stock solution

A vial was charged with PA (15 mg) and hydrated with milliQ H_2O (4.5 mL). The vial was shaken for 5 minutes.

Preparation of PC_{95} stock solution

For initial GNP growth, PC_{95} stock solution was prepared by dissolving PC_{95} (200 mg, 0.245 mmol) in minimal cyclohexane, which was immediately dried by rotary evaporation to give a thin film. H_2O (20 mL) was then added to the vial which was shaken 30 seconds. The cloudy solution was then sonicated for 15-20 min.

For PC_{95} solutions used with PA, vials were charged with varying masses of PC_{95} (i.e. - 2 x 6 mg, 12 mg, 18 mg, 24 mg and 2 x 30 mg respectively) and the PC dissolved in minimal cyclohexane. These were then rotary-evaporated to give thin films and rehydrated with milliQ H_2O (2 mL each). PA (500 μL) was charged into 5 vials of PC_{95} (1 x 6 mg, 12 mg, 18 mg, 24 mg and 1 x 30 mg respectively). The resulting solutions were sonicated in a bath sonicator for 15 minutes and all diluted with milliQ H_2O (to 17.5 mL each).

Preparation of chloride derived gold seed using PC

Gold chloride seed solution was prepared fresh before prior to each experiment. Briefly, to PC stock (1 mL) diluted to 5 mL with milliQ H_2O was added $HAuCl_4 \cdot xH_2O$ (10 mM,

125 mL), KBr (1.65 M, 7.5 mL) and while stirring vigorously, $NaBH_{4aq}$ (10 mM, 600 mL) was quickly added. The resulting purple seed solution was allowed to react 45 min to one hour prior to use.

Preparation of bromide derived gold seed using PC

Gold bromide seed solution was also synthesized fresh prior to each experiment. Briefly, PC stock (1 mL) was diluted to 5 mL with milliQ H_2O in a vial and while vigorously stirring, aqueous $HAuBr_4 \cdot xH_2O$ (10 mM, 125 μL) was added followed by immediate addition of $NaBH_{4aq}$ (10 mM, 300 μL). The resulting purple seed solution was allowed to react 5 min prior to use.

Preparation of growth solutions with KBr

A typical chloride growth solution was prepared by diluting PC stock (2 mL) with H_2O (15 mL). To this was added aqueous $HAuCl_4 \cdot xH_2O$ (10 mM, 400 μL), $KBr_{(aq)}$ (1.65M, 24.3 μL) and chloride derived lecithin gold seed (40 μL). The resulting orange solution was vigorously stirred and ascorbic acid (100 mM, 40 μL) was immediately and rapidly added. The solution immediately became transparent and then began to darken to a darker red/purple within 5 min. The resulting solution was allowed to react 18 h prior to analysis.

Preparation of growth solutions with $HAuBr_4$

A typical bromide growth solution was prepared by diluting PC stock (2 mL) with H_2O (15 mL). To this was added aqueous $HAuBr_4 \cdot xH_2O$ (10 mM, 400 μL), bromide derived

lecithin gold seed (40 μL). The resulting orange solution was vigorously stirred and a rapid addition of ascorbic acid (100 mM, 40 μL) was immediately performed. The solution immediately became transparent and then began to darken to a darker red/purple within 5 min. The resulting solution was allowed to react 18 h prior to analysis.

Centrifugation

Centrifugation was performed on a Sorvall RC-6 equipped with a SS-34 rotor. Samples were run at 3000 rpm (1068 x g) for 20 minutes and pellets collected and diluted to 1 mL.

Preparation of gel electrophoresis rig

Agarose (500 mg) was added to Tris – Boric Acid – EDTA (TBE) buffer (0.5 X, pH 8.4, 100 mL) and heated until agarose was uniformly dissolved. This was immediately poured into the chilled gel form and allowed to cool at 4ºC for 8-15 hours. The gel form is then transferred to the rig containing a Spectra/Por®RC Membrane (MWCO: 2-8,000). The rig was charged with TBE (0.5 X) buffer and the flow column connected to a paristaltic pump running at ~200 mL/hr. Lipid-coated GNPs were centrifuged to remove excess unbound lipids and concentrated down to a volume of 1 mL. These solutions were mixed with glycerol (20 μL) and loaded onto the gel. Gels were run at 300 V and fractions collected and analyzed by UV-Vis.

Preparation of KCN and sample dissolution

KCN was prepared freshly and used within 24 hours of preparation. KCN (200 mg) was dissolved in mQ H_2O (10 mL) to make a 307 mM solution. KCN (50 μL) was added to

each fraction of GNP solution off the gel and allowed to react 18 hours. Fractions were then frozen at -80 ˚C for 4 hours and lyophilized for 24 hours. A small amount of cyclohexane was introduced into each fraction to extract organic material from the salt and filtered and allowed to dry. MeOH (1 mL) was then used to dissolve the extract and MS analysis performed.

Instruments

Absorbance spectra are obtained on an Agilent 8453 UV-visible Spectrophotometer with a diode array using a 1.0 cm path length quartz cell. Transmission electron microscopy (TEM) images are acquired on a Tecnai F-20 FEI microscope. Images are collected at an acceleration voltage of 200 kV using a CCD detector. Samples are prepared by drop casting (5 μL) solutions of nanoparticles onto carbon-coated (300 Å) Formvar films on copper. Samples are dried for at least 1 h before images were obtained. For more dilute samples, multiple castings are performed on the same grid. Nanoparticle size analysis and length to width aspect ratio are performed using ImageJ software after applying a band pass filter to the images and adjusting the threshold. Mass Spectrometry samples were analyzed on a LTQ-Orbitrap mass spectrometer. The flow rate was set at 0.20 mL/min. Mobile phases consisted of 95:5 MeOH:H_2O and remained constant for each run. The injection volume was 20 μL. The mass spectrometer was operated under positive electrospray ionization with a voltage 4000 V in positive mode, the heater was set at 300 ˚C, the curtain gas (N_2) was kept constant at 50 psi. Quantitative analysis was monitored by total ion count and ESI results were analyzed on Xcalibur analysis software.

3.3 – Results and Discussion

$\underline{HAuCl_4}$ versus $\underline{HAuBr_4}$ in synthesis

PC contains a trimethylammonium headgroup similar to that of CTAB and long fatty-acid tail groups (Figure 3.1).

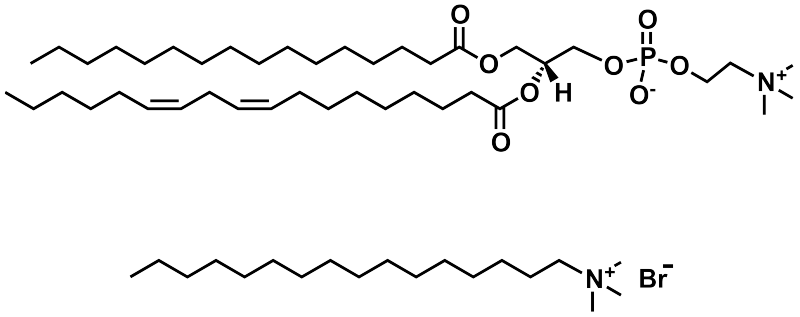

Figure 3.1 – Schematic of PC and CTAB. PC is depicted above with two tail groups off a glycerol linker while the PC makes up the head group. Note the similar headgroup to CTAB (bottom)

Using PC as our capping ligand, we started the synthesis using a yellow $HAuCl_4$ solution and reducing with ascorbic acid. This resulted in a blue solution of nanoparticles which immediately began aggregating out of solution. UV-Vis and TEM were taken, and as seen in Figure 3.2, only one plasmon band was seen in the UV-Vis spectrum. TEM (Figure 3.2) showed only spheres resulting from this particular synthetic technique.

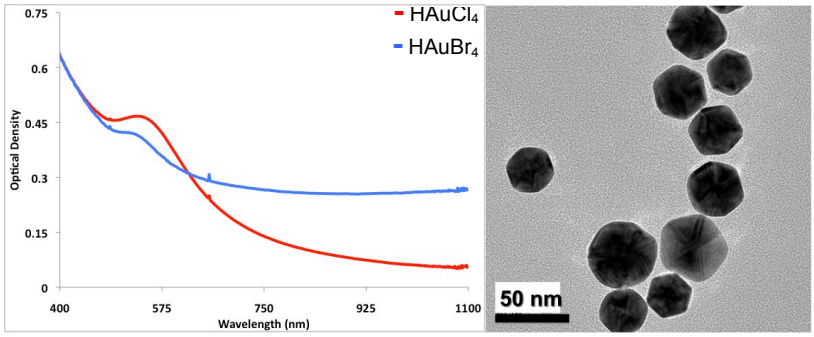

Figure 3.2 – UV-Vis spectrum and corresponding TEM of GNPs synthesized using $HAuCl_4$ in soybean extract. Red trace was taken with GNPs synthesized using $HAuCl_4$ in the growth solution and the blue trace using $HAuBr_4$

The use of $HAuCl_4$ gave only one plasmon band at 532 nm. The corresponding TEM had a scattering of anisotropic shapes, but an estimated 98% of the particles were spherical. This accounts for single plasmon band in the UV-Vis absorption spectrum. As we desired anisotropic shapes for our nanoparticles, we deduced that the Br^- was key in the shape control of nanoparticles. As CTAB is added to a solution of $HAuCl_4$, the solution turns a bright orange.

We found in previous studies that the shift in λ_{max} is due to bromide exchange.[116] It has been shown that the UV-Vis spectrum for the addition of CTAB to $HAuCl_4$ red-shifts as the bromide exchange takes place. This can be seen in Figure 3.1 in which we see the λ_{max} shifts from 295 nm to 390 nm. This indicates that anion exchange is indeed taking place. To support this, we added KBr to $HAuCl_4$ solutions and UV-Vis spectra taken of each addition (Figure 3.2).

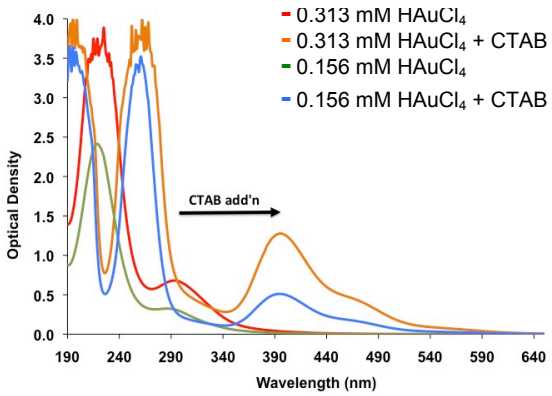

Figure 3.3 – UV-Vis spectra showing addition of CTAB to $HAuCl_4$

It can be seen that as the molar ratio of Br^- to Cl^- increases, the shift follows the same trend as that of CTAB addition. The λ_{max} red-shifts from 295 nm to 385 nm. We see that by 4x the molar ratio of KBr to $HAuCl_4$, that the λ_{max} has shifted to its maximum shift indicating a propensity of the bromide to coordinate to the gold(III) center.

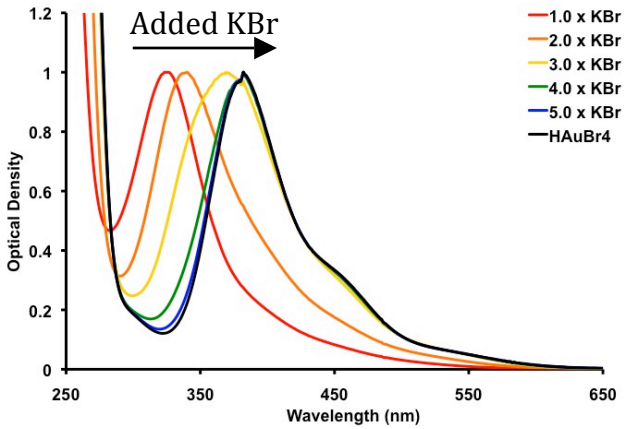

Figure 3.4 – UV-Vis spectra showing addition of KBr to $HAuCl_4$. Note all amounts are expressed in molar ratios of KBr to $HAuCl_4$ and all spectra are normalized (Find extinction for aucl and aubr)

Using $HAuBr_4$, we repeated the synthesis. The orange solution of $HAuBr_4$ was added to a lecithin solution and ascorbic acid used to reduce the gold. A red solution resulted and

UV-Vis and TEM were taken of the GNPs. Again, we see in Figure 3.5, only one plasmon band results at 532 nm from spherical nanoparticles, as seen in the adjoining TEM. Also, we see that the width of the plasmon band when performing a synthesis with $HAuCl_4$ is broader than that when using $HAuBr_4$. This leads to the color difference between the two solutions: Synthesis with $HAuCl_4$ being blue in color whereas a synthesis with $HAuBr_4$ is red.

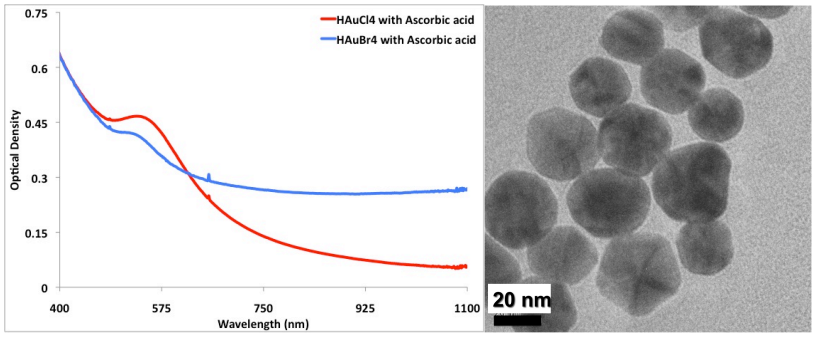

Figure 3.5 – UV-Vis spectrum and corresponding TEM of GNPs synthesized using $HAuBr_4$ in soybean extract

This, however, does not lead to anisotropic growth. It has been shown that seed mediated synthesis is needed for anisotropic growth.[52] In a typical growth, a seed solution is prepared using a strong reductant such as $NaBH_4$. The seeds are shown to give a nucleation point and the surfactant directs the one-dimensional growth.[57] It is believed the surfactant blocks growth on the {110} facet of the gold crystal giving growth in a one-dimensional direction.[137] This produces a majority of uniformly sized gold nanorods (Figure 3.7).

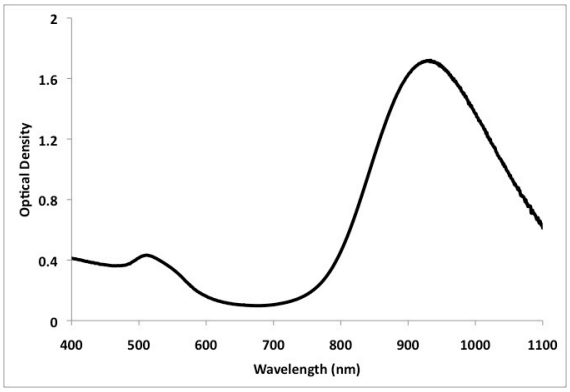

Figure 3.6 – UV-Vis of nanorods using CTAB as the capping agent. The nanorods have an average aspect ratio of 7. Note the ratio of the red-shifted plasmon to the blue-shifted plasmon.

Therefore we modified our synthesis incorporating a seed mediated method into our synthesis. Seeds were prepared using lecithin and $HAuBr_4$ and reduced using $NaBH_4$. Seeds were then introduced into our growth solutions and monitored by UV-Vis. Figure 3.7 shows a UV-Vis spectrum of the resulting growth solution. Along with the characteristic blue-shifted plasmon band at 532 nm, a second plasmon band is seen at 775 nm. This plasmon band is a result of anisotropic growth. This is one aspect that makes anisotropic growth desirable. Using UV-Vis spectroscopy, the reaction can easily be monitored. As growth of the longitudinal axis increases, the NIR plasmon band increases in intensity and red-shifts. As seen in a growth of CTAB (Figure 3.6), the intensity of the red-shifted plasmon band is much more intense than that of the blue-shifted plasmon band.

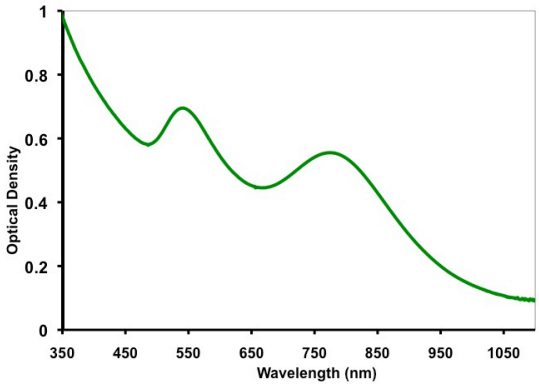

Figure 3.7 – UV-Vis spectrum of gold nanoparticles grown with $HAuBr_4$ and PC capping agent.

The growth of the nanoparticles in one dimension or two dimensions gives rise to the red-shifted plasmon band. The cross section of the nanoparticles is what is believed to give the blue-shifted plasmon band. Since rod-shaped GNPs have such a small cross sectional area, the oscillation of the electrons in the transverse band is stunted and therefore, a small absorption band is seen in the blue. Since our spectrum shows a larger blue-shifted absorption band, one of two (or both) scenarios are possible. We have a mixture of anisotropic nanoparticles, or we have different shapes than the rod-like nanoparticles. To confirm this, TEM was taken of the nanoparticles formed in the PC capped growth solution. As seen in Figure 3.8, a multitude of shapes are present on the TEM grid. A majority of the nanoparticles are spherical in shape, however, prismatic nanoplates, hexagonal nanoplates and rods are also dispersed throughout the sample.

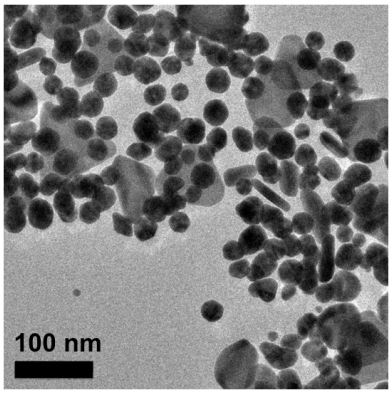

Figure 3.8 – TEM image of crude nanoparticle synthesis using $HAuBr_4$ and PC as a capping agent. Note the plethora of shapes and sizes.

This synthesis was also compared to a seed mediated synthesis in which $HAuCl_4$ and KBr were substituted in for $HAuBr_4$. As more KBr was added to the growth solution, you see a rise in intensity of the NIR plasmon band (Figure 3.10). There is also a shift of the plasmon band towards the red as the concentration of KBr increases from 4x the molar concentration of $HAuCl_4$ to 12x.

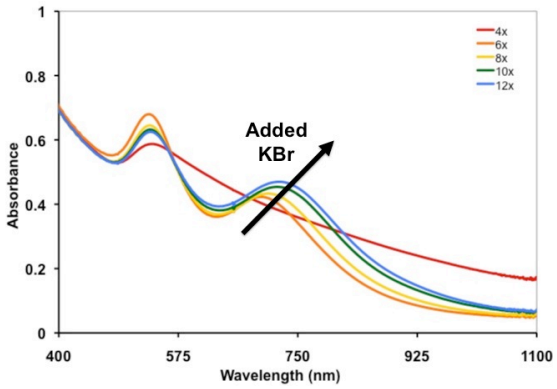

Figure 3.9 – UV-Vis spectra of KBr being added to seed mediated growth solution of PC and $HAuCl_4$.

This is further evidence that the bromide ion is needed for the growth of anisotropic

nanoparticles. As bromide is introduced to the growth solutions, the NIR (red-shifted) plasmon band appears and grows. However, as discussed later, the shapes found in the solution were not rod shaped GNPs as was initially believed.

Capping agent

CTAB is the standard capping agent for use in gold nanorod growth. However, it is not biocompatible. GNPs synthesized with CTAB therefore must be post-processed by coating the particles with polymers or ligand exchange performed to make the GNP more biocompatible.[152,153,154] Soybean PC is from a natural product and forms liposomes in aqueous media. These have a much higher propensity for compatibility in medicinal applications.

Thus far, we have discussed synthesis using a 30% PC (PC_{30}) extracted from soybeans. The idea that PC is a compatible substitute for CTAB from the similar structure of the ligands has been utilized for surface modification of GNPs.[65] We want to attempt shape controlled synthesis of GNPs from a biocompatible template. However, when we altered the synthesis to use a more pure form of soybean PC, we found some interesting results.

Using PC_{30} as the template allowed for a plethora of sizes and shapes of nanoparticles in the growth solution. In an attempt to narrow the shape distribution, a solution of 95% PC (PC_{95}) was substituted for PC_{30} in the synthesis. The resulting nanoparticles were analyzed by UV-Vis and TEM and compared to the corresponding nanoparticles synthesized from PC_{30} (Figure 3.11).

a)

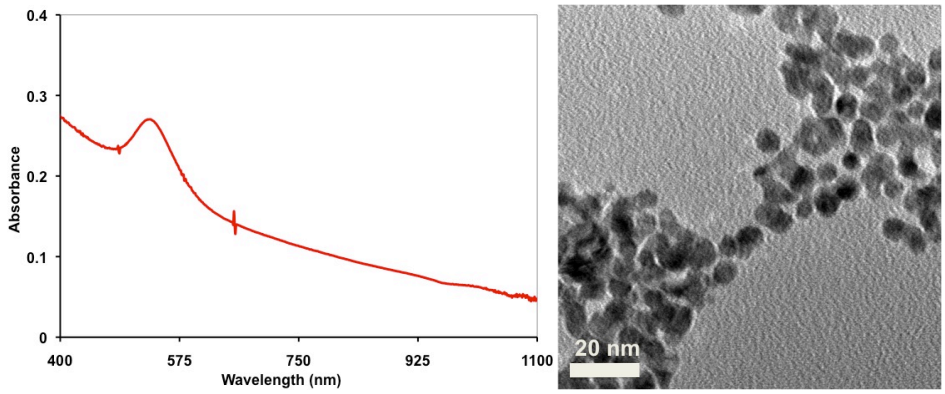

b)

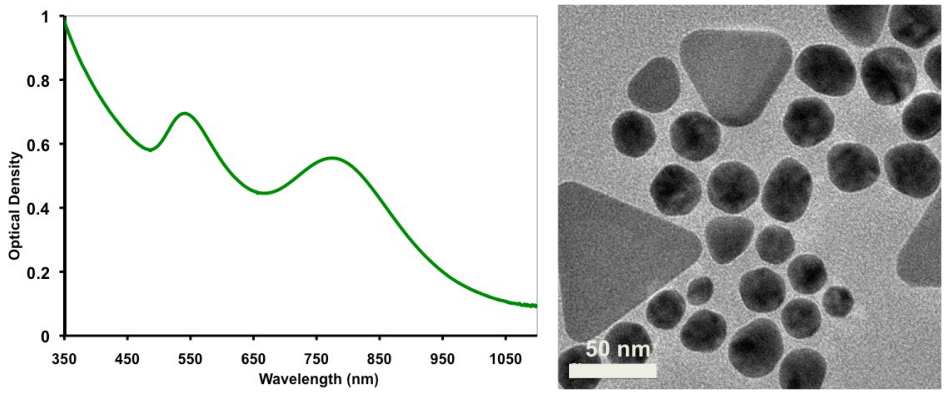

Figure 3.10 – UV-Vis and corresponding TEM of a) PC_{95} synthesis and b) PC_{30} synthesis respectively

As can be seen in Figure 3.11, a PC_{95}-GNP gives agglomerates of nanoparticles. The low intensity and scattering is evidence of aggregate formation in nanoparticles solutions and the TEM confirms that agglomerates of nanoparticles formed upon synthesis. This was also seen by the naked eye in the storage vial. Within 24 hours, a thin black precipitate could be seen in the bottom of the vial.

The single plasmon band absorption indicates that predominately only spherical particles form using PC_{95}. The breadth of the band is also broader than that of nanoparticles synthesized with PC_{30}. This is seen in the color of the growth solution as was also seen

when using $HAuCl_4$ in the synthesis above. The color of the solution was purple instead of red (Figure 3.11).

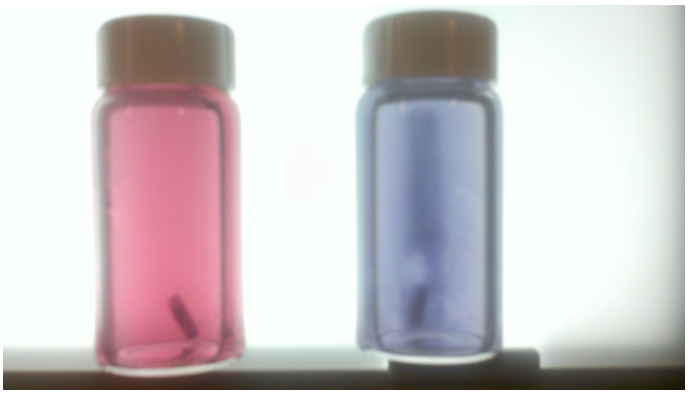

Figure 3.11 – Picture of vials containing PC_{30} growth (left) and PC_{95} growth (right). Note the precipitate in the PC_{95} sample

Due to this result, it is not believed that the PC is the component allowing for shape control. This will be discussed in a later section. However, this did lead to an added advantage in our synthetic technique.

Both PC_{95} and CTAB synthesized GNPs fell out of solution within an hour after synthesis. Using the soybean extract PC_{30} in the synthesis, however, increased the lifetime of the nanoparticles in solution up to six months when stored at 4˚C. Long shelf-lives of GNPs is very important when applying the nanoparticles to a medicinal use.

When using an impure natural product such as PC_{30} as a capping ligand for nanoparticles, it becomes more difficult to discern what materials are on the surface of the nanoparticle as compared to a synthesis using a pure compound (i.e. CTAB). This becomes especially

important when you consider shape control. One and two-dimensional growth of nanoparticles are usually driven by a number of particular components which block growth on specific crystal facets. CTAB, for example, blocks growth on the {110} facet allowing for one-dimensional growth of GNPs into rod-shaped nanoparticles.[52] Bromide was found to be required for directed growth, however contaminants such as iodide have been found to stunt growth of rod-shaped GNPs.[61]

PC_{30} contains a plethora of compounds that may have a role in the synthesis of anisotropic GNPs, particularly the nanoprisms seen above. Though the main components of PC_{30} are PC and phosphatidylethanolamine (PE), there are also small amounts of sterols, tocopherols and other plant byproducts, including dissociated fatty acids other phospholipids. Isolating the capping ligands is difficult

when solutions of GNPs contain all these compounds and separation is needed to seclude the specific ligands for identification. Traditionally, nanoparticles are separated using centrifugation at varying speeds to separate sizes, however shape separation is more difficult.

Our first thought was to identify the components in PC_{30} using HPLC-MS. We can then re-spike these components into growth solutions and test for plasmon absorption enhancement. We found that PC_{30} contained mostly lyso-PC and diacyl-PC components (Table 3.1). We then respiked many of these components into our growth solutions and monitored the growth by UV-Visible spectroscopy. However in every re-spike

experiment, we found that the component added degraded any anisotropic growth (Figure 3.12). Other components known to be in PC_{30}, which didn't show up on LC-MS such as cholesterol and sodium linoleate, were also spiked into growth solutions and also lead to degraded NIR plasmon band growth. Since this method was not proving fruitful, a more efficient approach to identifying the responsible ligand for anisotropy was employed using gel electrophoresis.

Table 3.1 – List of mass identities found in PC_{30}

Identity	Mass (m/z)	Retention time (min)
Lyso-EPC	578.4	2.2
Lyso-PPC	496.3	2.5
Triarachidicglyceride	947.3	3.5
Di-LPC	782.6	5.8
OLPC	784.6	7.4
POPC	760.6	9.5
SLPC	786.6	10.1
GPPC	788.6	13.1

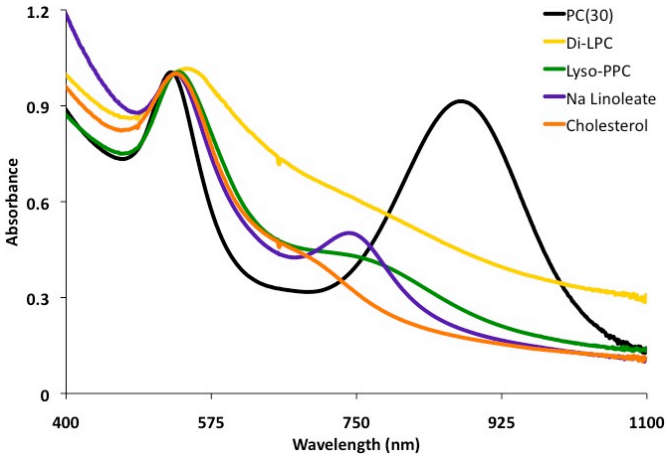

Figure 3.12 – UV-Vis spectrum showing resulting GNP traces after several components are spiked into a growth solution. The black trace is a normal growth solution without any spike.

Figure 3.13 shows a slab gel of our nanoparticles run at 200 V. UV-Vis and TEM show that the nanoprisms move slower through the gel and therefore analysis of the later fractions are essential in determining the capping ligand leading to the gold nanoprisms. The nanoparticles were then studied using UV-Vis, TEM and MS. Gel electrophoresis has previously been utilized to separate shapes of nanoparticles.[158,155] However, this wasn't attempted on any samples containing unknown ligands to our knowledge.

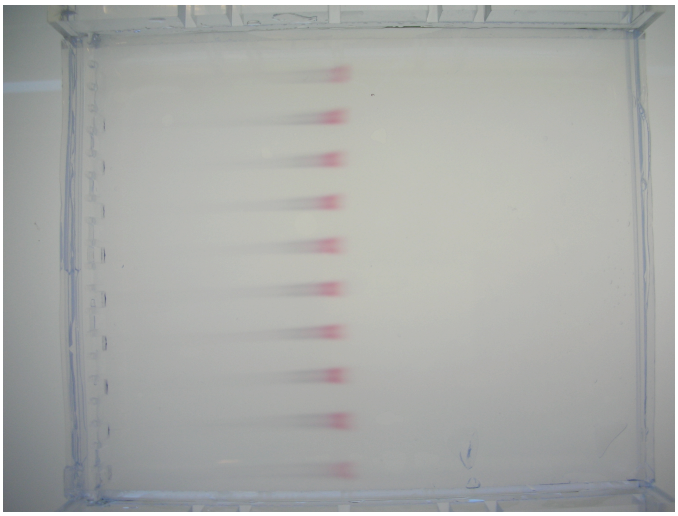

Figure 3.13 – Gel electrophoresis of anisotropic GNPs showing size and shape separation. Note the trailing of the bands as the plate-like nanoprisms are slower to move along the gel.

Discovering that shape separation was possible, we utilized a gel prep column to collect fractions as they came off the gel and analyzed the fractions using TEM (Figure 3.14). It was also seen that the nanoprisms were single crystalline and equilateral in geometry (Figure 3.15). These factors are important in respect to the optical properties of the

GNPs.[156] The resulting plasmon absorptions of each fraction were monitored by UV-Vis and an NIR plasmon absorption was seen growing as the fractions progressed (Figure 3.15). We found that nanoprisms increase in population leading to an increase in the NIR plasmon band intensity in later fractions. Upon realizing this, we leached the GNPs from the capping ligand using KCN and extracted the organic ligands, using LTQ-OrbiTrap MS to analyze the makeup of these ligands.

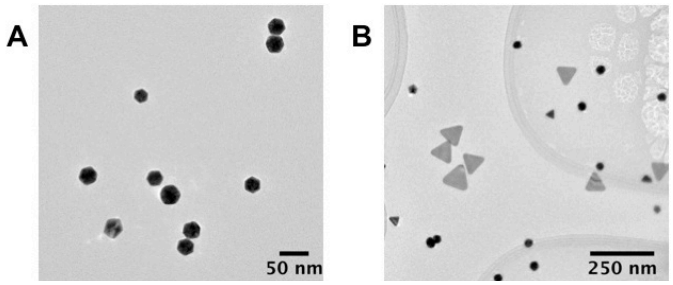

Figure 3.14 – A. Particles from front of gel band show only GNPs of a semi-uniform size B. Particles from tail of gel band show a multitude of nanoprisms, though there are still some smaller nanoparticles present

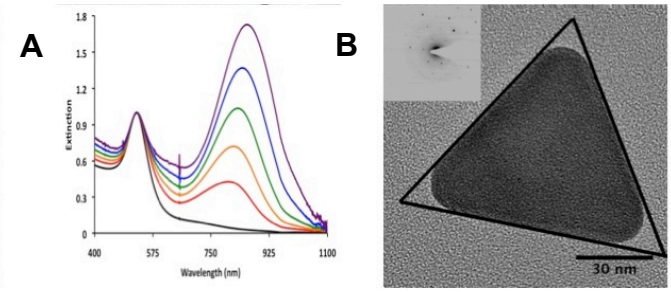

Figure 3.15 – A. A UV-Vis analysis of several fractions from the column revealing a steady increase of the NIR absorption band (normalized at 532 nm). B. High resolution TEM showing uniform crystal lattice and SAED inset showing [111] zone axis with {220} diffraction spots. TEM also allows us to analyze the

geometry of a gold nanoprism and show that it is equilateral.

Mass spectra show peaks corresponding to phosphatidic acid (PA) at 669.86 m/z (Figure 3.16). This peak can be calculated as a PA ligand containing fatty acid tail groups of C 16:0 and C 18:3. MS^2 was attempted to confirm these tail groups, however the C 16:0 tail was the only peak to occur and was never consistent enough for positive identification. Though positive analysis of the exact ligand escaped us, we incorporated a sample of PA into our synthesis.

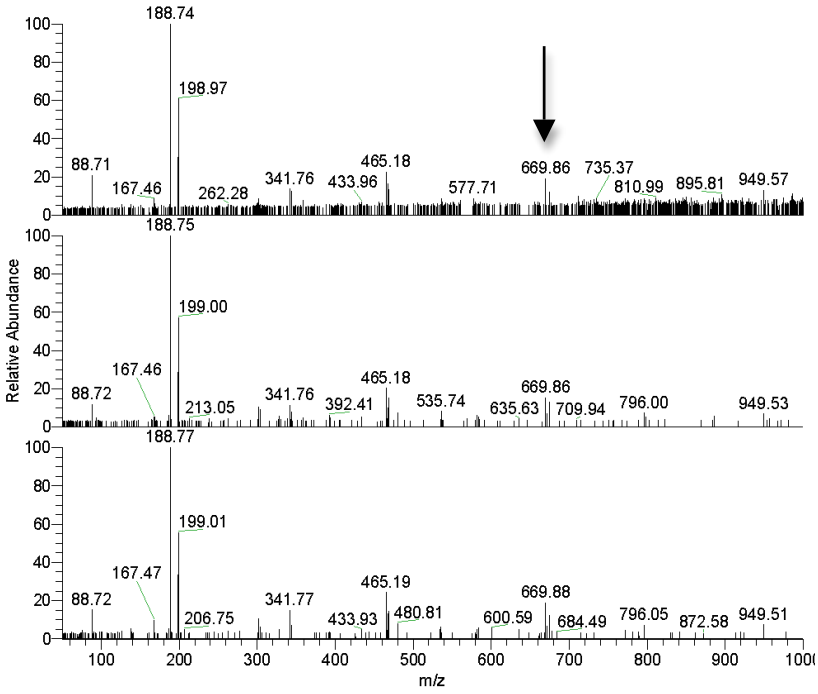

Figure 3.16 – Mass spectrum of 3 concurrent fractions from a gel prep column showing a growth of the peak at 669.86 m/z.

PA from egg yolk was spiked into PC_{30} and PC_{95} stock solutions prior to sonication in order for it to be incorporated into the liposomes. Although PC_{30} growth solutions

produced little difference in the NIR plasmon band when spiked with PA, PC_{95} showed a steady growth of an NIR plasmon band when PA was added to the system in consecutively larger amounts (Figure 3.17). In other words, as the ratio of PC_{95} to PA was decreased, a NIR plasmon band appeared and increased leading us to conclude that PA is essential in the growth of gold nanoprisms. As seen above, PC_{95} never produced nanoprisms or an NIR plasmon band. Another observation was the sharpening of the blue-shifted plasmon band. This indicates decreasing aggregation in the solution.

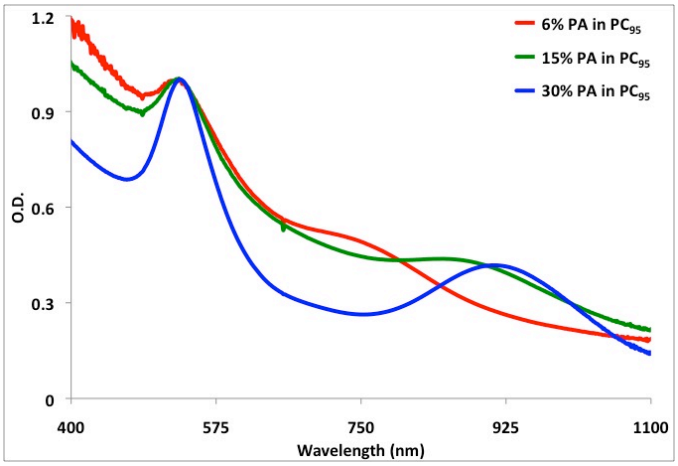

Figure 3.17 – UV-Vis of varying ratios of PA to PC_{95}. The higher the ratio of PA to PC_{95}, the larger the intensity of the NIR plasmon band and the sharper the blue-shifted plasmon band.

The source of the PA lipid is unknown. MS analysis of the original PC_{30} does not show any sign of PA, though many other phospholipid compounds are present. The appearance of PA could be due to a surface reaction occurring in the initial steps of the reaction, however, this is hypothetical and we have not found the source of the PA appearance.

3.4 – Conclusion

We have shown that anisotropic nanoparticles can be synthesized using soybean extract and $HAuBr_4$. The soybean extract has the advantage of being biocompatible as well as being cheap and readily available. It has also been demonstrated that bromide play a key role in the anisotropy of GNPs during synthesis. This can be seen when spiking samples of $HAuCl_4$ with KBr. Substituting $HAuBr_4$ for $HAuCl_4$ enhances the synthesis giving more intense NIR-shifted plasmon bands. The resulting solutions are stable for months at a time and show promise for use in medicinal applications. However, this is not a result of the PC as we initially believed. Although, PC_{30} produces a relatively large population of prismatic GNPs, PC_{95} shows poor shape control as well as immediate aggregation out of solution. PA was identified as a critical component of the capping ligands on gold nanoprisms. Using gel electrophoresis, it was found that we could increase the nanoprisms population of our GNP solutions and mass spectrometry could be used to identify PA. Spiking PA into PC_{95} growth solutions revealed an NIR plasmon band indicative of anisotropic GNPs. As the ratio of PA to PC_{95} increased, so did the intensity of the red-shifted plasmon band. This is the first instance of the use of PA to grow anisotropic GNPs that we have seen. More experiments are being performed to discern the extent of the shape control of PA in seed mediated growth of gold nanoprisms.

Shape-directing agents are of great importance in nanotechnology when considering GNP use in therapy. However, identifying a specific ligand responsible for shape-control in a conglomerate of components can be a challenge. Gel electrophoresis is mainly used in biology and biochemistry to separate biological molecules such as oligonucleotides and

protein strands.[157] These molecules can be digested to break bonds and give the make-up of the strands in question. Other pre-processing may be required for proteins such as denaturing the molecule with sodium dodecyl sulfate (SDS) to apply a charge for carrying the molecule down the gel. When a current is applied to the gel, the molecules are carried down the gel according to size and charge and separated giving bands that can be applied to specific sequences allowing for qualitative analysis.[157]

Using this data, it was theorized that nanoparticles could also be separated according to size and shape.[158] Hanauer *et al.* separated silver and gold nanoparticles by size and shape successfully and analyzed the separated particles using UV-Vis and TEM. The bands elucidated a good separation according to shape and TEM confirmed that shape separation is possible for rod-shaped and spherical shaped GNPs.

Using a Biorad preparatory gel rig, we performed a separation of GNPs and analyzed our success using UV-Vis and TEM. We see a large increase in the number of triangular gold nanoplates after separation. Fractions were taken off the gel and the resulting GNP fractions were dissoluted with KCN and lyophilized. The fractions were extracted with organic solvent to remove salts and analyzed using MS.

Cyanide Permeability of Gold Nanoprism Edges

4.1 – Thiol

Introduction

Cyanide leaching has been used in mining since 1887 for the extraction of gold.[159] Cyanide forms a linear gold complex and allows it to become water soluble, giving feasibility to extracting gold from the ore. The process uses oxygen as well as seen by

$$4Au + 8NaCN + O_2 + 2H_2O \rightarrow 4Na[Au(CN)_2] + 4NaOH$$

Nanoparticle synthesis from naturally occurring lipids are fitting due to the diversity of their chemical structures. The lipids have advantages over other complexes of forming complex three-dimensional structures, being available from renewable food stocks and allowing for an inexpensive source of the complexes, such as soy.[160,166] Nanoparticles synthesized from the natural lipids have the added advantage of acting as models for cell membrane interactions[161] and are useful as likely biocompatible probes.[162]

Stability of GNPs is especially important when using the nanoparticles in biological systems.[166] Any aggregation of the particles can lead to adverse effects in the bio-system. The stability of GNPs has been studied extensively in both organic-soluble[163] and water-soluble systems.[166] To improve stability of these GNPs, hybrid capping agents have been employed such as alkanethiols,[166] which act both as an anchor for the lipids and as a protectorant for areas of high curvature on the GNP. This is similar to the role

alkanethiols play in two-dimensional hybrid bilayers[164] as well as in tethered bilayer lipid membrane systems.[165]

This makes cyanide ideal for testing the protective capability of capping ligands on GNPs in aqueous solutions. We report here on the use of cyanide in the stability of soy lecithin as well as the stability of a soy lecithin/decanethiol hybridized capping agent.

4.2 – Experimental

L-α-Phosphatidylcholine Type IV-S ≥ 30% TLC (PC_{30}), L-ascorbic acid, potassium cyanide and 1-decanethiol were purchased from Aldrich. Hydrogen tetrabromoaurate (III) hydrate was purchased from Strem Chemicals Inc. Sodium borohydride (98%) was purchased from J.T. Baker. Milli-Q H_2O was used at 18.1 mΩ resistance. Centrifugation was performed on a Beckman Optima LE-80K Ultracentrifuge equipped with a SW65K swinging bucket rotor at 4000 rpm (1592 x g RCF).

Preparation of bromide derived gold seed using PC_{30}

Gold bromide seed solution was also synthesized fresh prior to each experiment. Briefly, PC_{30} stock (1 mL) diluted to 5 mL with milliQ H_2O was added to a vial and while vigorously stirring, aqueous $HAuBr_4 \cdot xH_2O$ (10 mM, 125 μL) was added followed by immediate addition of $NaBH_{4aq}$ (10 mM, 600 μL). The resulting purple seed solution was allowed to react 45 min to one hour prior to use.

Preparation of growth solutions with $HAuBr_4$

A typical bromide growth solution was prepared by diluting PC_{30} stock (2 mL) with H_2O (15 mL). To this was added aqueous $HAuBr_4 \cdot xH_2O$ (10 mM, 400 μL), bromide derived lecithin gold seed (40 μL). The resulting orange solution was vigorously stirred and a rapid addition of ascorbic acid (100 mM, 40 μL) was immediately performed. The solution immediately became transparent and then began to darken to a darker red/purple within 5 min. The resulting solution was allowed to react 18 h prior to analysis.

Preparation of decanethiol

Decanethiol was prepared by dissolving 1-decanethiol (20.6 μL) in 95% ethanol (1 mL) to make a 100 mM solution. A 10 μM solution was prepared similarly. Both concentrations of 1-Decanethiol were added to separate 1 mL aliquots of GNP growth solution and UV-Vis taken while stirring gently.

Preparation of KCN

KCN was prepared freshly and used within 24 hours of preparation. KCN (200 mg) was dissolved in mQ H_2O (10 mL) to make a 307 mM solution. 10 μL was added to each solution of GNP growth solution and GNP/1-decanethiol hybrid solution respectively (@ 1 mL each). The dissociation of gold from the nanoparticle was monitored by UV-Vis over time. Spectra were taken at t=0 s, t=10 s and t=60 s while stirring gently.

Instruments

Absorbance spectra are obtained on an Agilent 8453 UV-visible Spectrophotometer with a diode array using a 1.0 cm path length quartz cell and a magnetic stirring mechanism.

TEM

TEM images are acquired on a Tecnai F-20 FEI microscope. Images are collected at an acceleration voltage of 200 kV using a CCD detector. Samples are prepared by drop casting (5 μL) solutions of nanoparticles onto carbon-coated (300 Å) Formvar films on copper. Samples are dried for at least 1 h before images were obtained. For more dilute samples, multiple castings are performed on the same grid. Nanoparticle size analysis and length to width aspect ratio are performed using ImageJ software after applying a band pass filter to the images and adjusting the threshold.

4.3 Results and Discussion

Previous work has been performed on spherical GNPs using several thiols as a stabilizing agent.[166] Thiols have been shown to improve stability of nanoparticles by coordinating to any exposed gold surface such as edges and areas of high curvature. These areas of high curvature allow access to low cone angle detergents such as saturated thiols and this in turn lowers the strain energy of the PC bilayer around the curvature.[166,167]

A simplified schematic is shown in Figure 4.1 showing thiol coverage on the surface of the GNPs while the organic tail groups are protected from the aqueous solution by the

soy lipid bilayer. Figure 4.1 also gives and example of two substances with differing cone angles. This affects the ability of the lipid to cover the surface of the nanoparticle due to ineffective packing of the lipids. High strain energies can be induced if capping agents with large cone angles are packed on a highly curved surface.

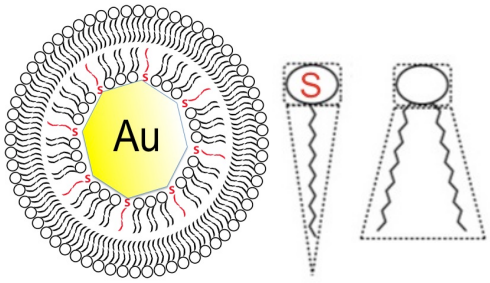

Figure 4.1 – Schematic of thiol-hybridized liposome and the comparison of cone angle for the thiol versus the phospholipid component of the lecithin

Using 1-decanethiol as a co-capping agent, we tested several concentrations of thiol to determine the stability of the GNPs to cyanide leaching. This was monitored by UV-Visible spectroscopy at several time increments. Figure 4.2 shows a series of spectra obtained by adding KCN to a simple growth solution. We see that the soy lecithin does not give full coverage of the surface of the nanoparticles as is demonstrated by the loss of the red-shifted plasmon absorption signal and the greatly decreased intensity of the blue-shifted plasmon band within a minute.

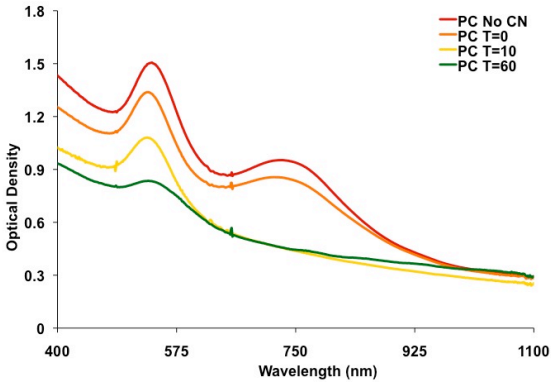

Figure 4.2 – Addition of KCN to 1 mL of our PC growth solution. Time increments are at 0, 10 and 60 seconds. The red-shifted plasmon intensity decreases showing the inability of PC to provide protection to the anisotropic nanoparticles whereas the blue-shifted intensity does decrease, but never disappears

The blue-shifted plasmon band does not completely disappear, even after 24 hours so there are some particles that do have complete coverage and are resistant to CN etching. TEM were taken of the remaining solution of particles and these are seen in Figure 4.3, which reveals that the nanoparticles are extremely small (< 10 nm).

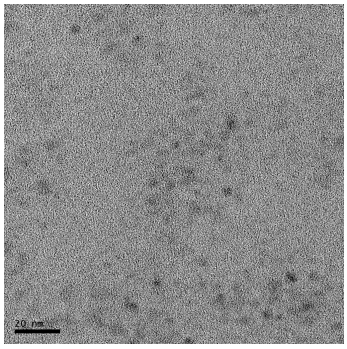

Figure 4.3 – TEM of particles remaining 4 hours after cyanide etching of the growth solution. Particle sizes are < 10 nm.

First, 100 mM 1-decanethiol was added to a gold growth solution until the UV-Vis shows a slight formation of aggregates (occurred at 9 μL). This creates a saturated thiol solution with an overall thiol concentration of 890 μM. This ensures that all exposed surface should be covered in thiol. The aggregation occurring is believed to be due to the exchange of phospholipid with thiol and causing them to fall out of solution from reduced solubility. This also causes an initial intensity drop when thiol is added as seen in Figure 4.4.

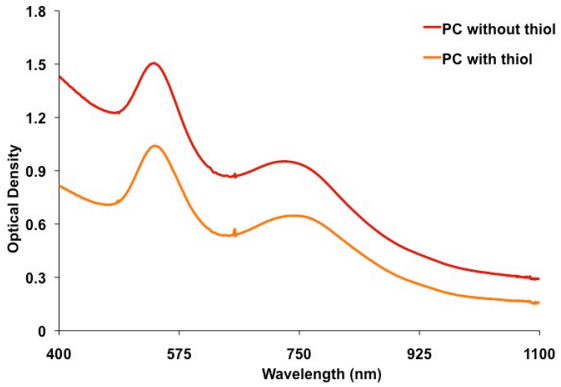

Figure 4.4 – UV-Vis spectra of PC growth solution with (orange trace) and without (red trace) 1-decanethiol added

To test the stability of the resulting hybrid nanoparticles, KCN was added and the solution was monitored by UV-Vis. Figure 4.5 shows the resulting UV-Vis spectral series.

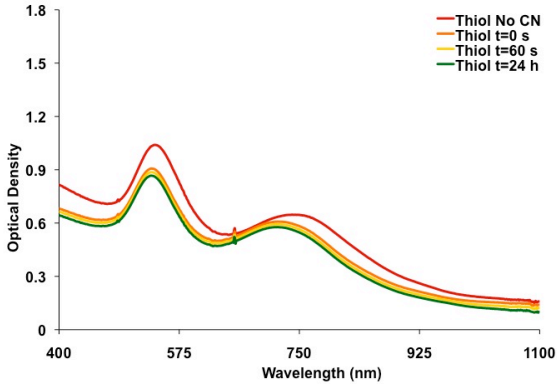

Figure 4.5 – Thiol hybridized GNPs before (red) and after addition of KCN.

We can see in Figure 4.5 that no decrease in intensity occurs after the initial addition of the KCN. The stability of the nanoparticles is such that after 24 hours, the solution still gives a UV-Vis signal showing both plasmon bands (Figure 4.5, green trace). In order to test the stability of the different shapes seen in the PC growth solution, we added 20 μL of 10 mM thiol solution giving a final concentration of 200 μM. When we add cyanide to this solution, we find that there is an initial drop in intensity that continues for 30 minutes. We see that after 2 minutes, the red-shifted plasmon band disappears completely and the blue-shifted plasmon band remains even after 30 minutes. As seen with the PC sample above, this is indicative of spherical particles surviving the leaching process. Figure 4.6 shows the progression of the λ_{max} for both the red-shifted and blue-shifted plasmon bands.

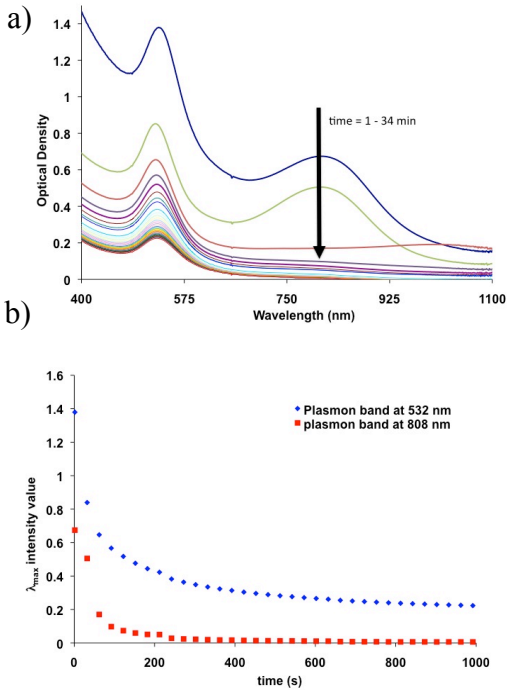

Figure 4.6 – a) UV-Vis showing progression of hybrid nanoparticles after cyanide addition. Each trace is a 1-minute time increment. b) This graph shows the value of the λ_{max} for both the red-shifted (red trace) and blue-shifted (blue trace) plasmon bands

Figure 4.6 shows that the prismatic nanoparticles are much less stable to cyanide etching than the spherical nanoparticles in our solution. The red-shifted plasmon band disappears within 2 minutes while the blue-shifted plasmon band remains for multiple days. It is believed that the high area of curvature on the edge of our prismatic nanoparticles and the chemical makeup of the lipids on the edge allow easy access for cyanide, even with thiol addition. High strain energy of the lipids is associated with the high amount of curvature on the GNPs. This can be alleviated using alkane thiol. In spherical GNPs, we think that the alkyl group of 1-decanethiol excludes a volume of lipid from the inner leaflet, thereby reducing the strain energy associated with a highly curved lipid layer.[168] However, in a

prismatic GNP, the bilayer coverage of the prismatic nanoparticle's edge does not seem to be complete and even with thiol as a stabilizing agent, the gold surface remains exposed (Figure 4.7).

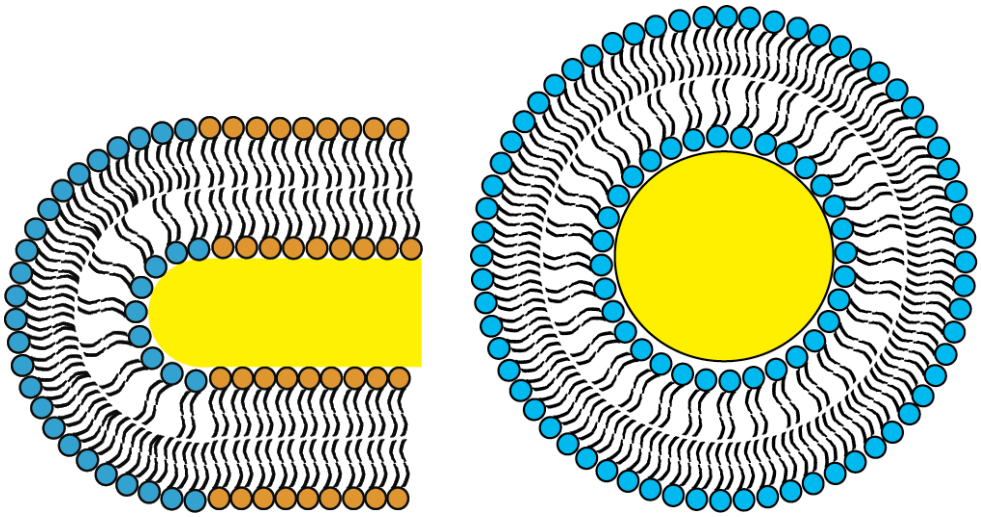

Figure 4.7 – Schematic showing degree of curvature of lipids on a prism's edge versus a spherical nanoparticle's edge. The degree of curvature of a prism's edge is much sharper leaving more room between the lipid's inner layer for cyanide penetration.

Conclusion

We've shown the dependence of 1-decanethiol concentration on the stability of prismatic and spherical GNPs. It is seen that at lower concentrations, the edges of the prismatic GNPs are exposed to KCN attack and dissociate within minutes. This can be useful in explaining the stability and effectiveness of these nanoparticles in when used in the design of biosensors as well as providing a method of etch resists for gold micropatterning. Additionally, this data can help contribute to our understanding of how these systems can be used for drug delivery.

Conclusions and Recommendations for Future Work

The work presented in my dissertation describes the synthesis, analysis, purification and modification of a prismatic gold nanoparticle for potential use in biological systems. Using soybean lecithin and $HAuBr_4$ in a seed mediated synthesis produced a mixed population of prismatic gold nanoparticles and spherical gold nanoparticles, which could be separated using gel electrophoresis and analyzed using mass spectrometry. Phosphatidic acid was found to be responsible in part for the shape control of the GNPs and the stability of the GNPs in water was achieved and improved upon using thiol addition. The experiments discussed in this thesis have led to new insights in gold nanoparticle growth.

Conclusion 1

Growth conditions are important when considering shape control of GNPs in an aqueous environment. Halide composition showed us that bromide salts of gold were found to be critical in shape control of GNPs. When titrating bromide salt into a growth solution containing soy lecithin and $HAuCl_4$, the growth of a NIR plasmon band is revealed. Substituting $HAuBr_4$ enhances the NIR plasmon band to a local maximum absorption. The ligand source was also shown to be critical in GNP growth. While, PC_{30} shows anisotropic growth, PC_{95} reveals the phosphatidylcholine is not the responsible ligand for shape control. PC_{95} also reduced the stability of GNPs in solution, causing aggregation almost immediately after synthesis, however, PC_{30} allows for stability of GNPs for multiple months following synthesis.

Conclusion 2

Gel electrophoresis was the most effective means of size and shape separation of GNPs available to us. Using a gel prep column, we could partially separate our prismatic GNPs from the larger part of the spherical GNPs. TEM analysis of the prismatic GNPs shows an average size of 94 nm and that the GNPs are single crystalline. UV-vis shows the final fractions giving a λ_{max} at 865 nm. Leaching the gold using KCN and extracting the ligands allowed analysis using MS and identification of phosphatidic acid as a potential shape-directing ligand. Upon spiking PC_{95} (known not to give anisotropic GNPs) with PA, it was indeed found that a NIR plasmon band grows into the UV-Vis. This is also the first instance of synthesis of anisotropic GNPs using PA that we have found.

Future Work

A more efficient separation of the shapes of GNPs would allow for a more detailed analysis of the surface ligands found on the prismatic GNPs. This would in turn lead to a more efficient synthesis of prismatic GNPs and maximize the yield of prismatic GNPs. Possible solutions to the separation problem would be to increase the length of the gel column and decrease the voltage to allow more time to separate. Other techniques such as membrane permeation and nanofiltration were not extensively pursued and are also viable separation techniques.

More PA titration experiments are currently under way. As the limited time and limited amount of PA in the lab prevented us from including that work in the dissertation, it is still being studied for publication.

Conclusion 3

Stability of GNPs is paramount when considering their use in biological systems. The biological environment contains a large array of components that could lead to degradation or aggregation of GNPs in the system. In adding small amounts of decanethiol to the GNPs, we found that we could study the stability of the GNPs to cyanide etching. It was found that at 5 μM concentration of decanethiol, both the spherical and prismatic GNPs were completely impermeable to cyanide. If the concentration of thiol was lowered to 2 μM, the prismatic GNPs were found to lose their stability to cyanide while the spherical GNPs retained their protection. This experiment led to a better understanding of the ligand coverage on the surface of the different shapes of GNP. It is postulated that the coverage of soy ligand on the edge of the prismatic GNPs is not sufficient to prevent permeation of cyanide to the gold surface. However, a sufficient amount of decanethiol prevents this permeation allowing for a possible protective barrier when introduced into a biological system.

Future work

These experiments were done prior to our work in the separation of the GNPs. A more uniform population of prismatic GNPs would allow us to get a better idea of what is occurring at the gold surface and also allow us to compare different shapes and sizes of GNPs to cyanide etching both with and without thiol. This work also shows potential in allowing a specific shape to be leached and the ligand content of those shapes to be analyzed by MS. In other words, if we stabilize only the spherical GNPs to cyanide and dissolve the prismatic GNPs, the free ligand's content in solution could be analyzed and

provide another method for the identity of shape-directing ligands.

References

[1] Faulkner, Raymond Oliver (1962). *A Concise Dictionary of Middle Egyptian* (11th ed.). Oxford, United Kingdom: Griffith Institute. p. 129.

[2] W. Ostwald (1917) *An Introduction to Theoretical and Applied Colloid Chemistry*. John Wiley & Sons, Inc. New York.

[3] P.C. Ray (1903). *History of Hindu Chemistry, The Bengal Chemical and Pharmaceutical Works*. Calcutta.

[4] British Museum, http://www.britishmuseum.org/explore/highlights/highlight_objects/pe_mla/t/the_lycurgus_cup.aspx

[5] Harden D.B. and Toynbee J.M.C. (1959) *The Rothschild Lycurgus Cup*. Archaeologia, Vol. 97.

[6] Susan Frank (1982). *Glass and Archaeology*. London.

[7] Kunckle, Johann (1679). Ars vitraria experimentalis, oder, Vollkommene Glasmacher-Kunst (Documenta technica) (German Edition). Brandenburg.

[8] Michael Faraday, *Philos. Trans. R. Soc. London*, **1857**, *147*, 145.

[9] R. Zsigmondy. (1917). *The Chemistry of Colloids*, John Wiley & Sons, Inc., New York.

[10] R. Zsigmondy. (1909) *Colloids and the Ultramicroscope*. John Wiley & Sons, Inc. New York.

[11] Zsigmondy, R. Huckel, E. *Zeitschrift Fur Physikalische Chemie—Stochiometrie Und Verwandtschaftslehre.* **1925**, *116*, 291.

[12] R. Zsigmondy, Colloids and the Ultramicroscope, John Wiley & Sons, Inc., New York, 1909.

[13] T. Svedberg. (1921) *The Formation of Colloids.* D. Van Nostrand Company, Inc. New York.

[14] T. Svedberg, A. Tiselius. (1928) *Colloid Chemistry*, The Chemical Catalog Company, Inc. New York.

[15] T. Svedberg, K.O. Pedersen. (1940) *The Ultracentrifuge*, Oxford University Press. Oxford.

[16] Chanda N., Kan P., Watkinson L., Shukla R., Zambre A., Carmack T., Engelbrecht H., Lever J., Katti K., Fent G., Casteel S., Smith C. J., Miller W., Jurisson S., Boote E., Robertson D., Cutler C., Dobrovolskaia M., Kannan R., Katti K. V. *Nanomedicine*, **2010**, *6*, 201.

[17] Corma, A., Garcia, H. *Chem. Soc. Rev.*, **2008**, *37*, 2096.

[18] Hasobe, T., Imahori, H., Kamat, P. V., Ahn, T. K., Kim, S. K., Kim, D., Fujimoto, A., Hirakawa, T., Fukuzumi, S. *J. Am. Chem. Soc.*, **2005**, *127*, 1216.

[19] Kean, W. F. Kean, I. R. L. *Inflammopharmacology*, **2008**, *16*, 112.

[20] Wiegleb, J. C. (1777). Historisch-Kritische Untersuchung Der Alchemie. Zental-Antiquarit, Der Deutschen Demokratischen Republik, Leipzig.

[21] *The New Jerusalem Bible*. Ed. Susan Jones. New York: Doubleday, 1985. Print. Exodus 32:20.

[22] Waley, A. (1956). *The Way and Its Power: A Study of the Tao Teaching and its place in Chinese Thought*. Allen and Unwin, London.

[23] Fung, Y. L. (1952). *A History of Chinese Philosophy*. Translated by Derk Bodde. Vol. 1, Ch 8.

[24] Garrison F. H. (1966) *Introduction to the History of Medicine*, 4th ed. Philadelphia: W. B. Saunders, 112.

[25] Hunt, L. B. *Ambix.*, **1979**, *26*, 221.

[26] Koch, R. Deutsche medinische Wochenschrift, **1890** 16, 756.

[27] Forestier, J. *Annales de medicine Intern Societe medical Des Hopitaux de Paris Bulletins et Memoires*, **1930**, *54*, 272.

[28] Giljohann, D. A., Seferos, D. S., Daniel, W. L., Massich, M. D., Patel, P. C. Mirkin, C. A. *Angew. Chem. Int. Ed.*, **2010**, *49*, 3280.

[29] Huang, X. Jain, P. K., El-Sayed, I. H., El-Sayed, M. A. *Lasers Med. Sci.*, **2008**, *23*, 217**.**

[30] Ah, C. S., Hong, S. D., Jang, D. *J. Phys. Chem. B*, **2001**, *105*, 7871.

[31] Huang, X., El-Sayed, I. H. Qian, W.El-Sayed, M. A. *J. Am. Chem. Soc.*, **2006**, *128*, 2115.

[32] Cherukuri, P., Glazer, E. S., Curley, S. A. *Adv. Drug Delivery Rev.*, **2010**, *62*, 339**.**

[33] Alkilany, A. M., Thompson, L. B., Boulos, S. P., Sisco, P. N., Murphy, C. J. *Adv. Drug Delivery Rev.,* **2012**, *64*, 190**.**

[34] Lin, K. Y., Bagley, A. F., Zhang, A. Y., Karl, D. L., Yoon, S. S., Bhatia, S. N. *Nano LIFE*, **2010**, *1*, 277.

[35] Sekhon, B. S. *J. Pharm. Sci.*, **2012**, *2*, 14.

[36] Huff, T. B., Tong, L., Zhao. Y., Hansen, M. N., Cheng, J., Wei, A. *Nanomedicine*, **2007**, *2*, 125.

[37] El-Sayed, I. H., Huang, X., El-Sayed, M. A. *Cancer Letters*, **2006**, *239*, 129.

[38] Rai, A., Singh, A., Ahmad, A., Sastry, M. *Langmuir*, **2006,** *22,* 736.

[39] Hirsch, L. R., Stafford, R. J., Bankson, J. A., Sershen, S. R., Rivera, B., Price, R. E., Hazle, J. D., Halas, N. J., West, J. L. *PNAS*, **2003**, *100*, 13549.

[40] Shankar, S. S., Rai, A., Ankamwar, B., Singh, A., Ahmad, A., Sastry, M. *Nat. Mat.*, **2004**, *3*, 482.

[41] Au, L., Zheng, D. Zhou, F., Li, Z., Li, X., Xia, Y. *ACS Nano*, **2008**, *2*, 1645.

[42] Hurst, S. J., Payne, E. K., Qin, L., Mirkin, C. A. *Angew. Chem., Int. Ed.* **2006**, *45*, 2672.

[43] Jin, R., Cao, Y., Mirkin, C. A., Kelly, K. L., Schatz, G. C., Zheng, J. G. *Science* **2001**, *294*, 1901.

[44] Millstone, J. E., Park, S., Shuford, K. L., Qin, L., Schatz, G. C., Mirkin, C. A. *J. Am. Chem. Soc.* **2005**, *127*, 5312.

[45] Tao, A. R., Habas, S., Yang, P. *Small* **2008**, *4*, 310.

[46] Xia, Y., Xiong, Y., Lim, B., Skrabalak, S. E. *Angew. Chem., Int. Ed.* **2009**, *48*, 60.

[47] Zhou, K., Li, Y. Ibid.**2012**, *51*, 602.

[48] Somorjai, G. A., Frei, H., Park, J. Y. *J. Am. Chem. Soc.* **2009**, *131*, 16589.

[49] Giljohann, D. A., Seferos, D. S., Daniel, W. L., Massich, M. D., Patel, P. C., Mirkin, C. A. *Angew. Chem., Int. Ed.* **2010**, *49*, 3280.

[50] Yu, Y., Chang, S., Lee, C., Wang, C. R. C. *J. Phys. Chem. B* **1997**, *101*, 6661.

[51] Mohamed, M. B., Ismail, K. Z., Link, S., El-Sayed, M. A. *J. Phys. Chem. B*, **1998**, *102*, 9370.

[52] Jana, N. R., Gearheart, L., Murphy, C. J. *Chem. Mater.* **2001,** *13,* 2313.

[53] Jena B. K., Raj C. R. *J. Phys. Chem. C* **2007,** *111,* 15146.

[54] Nehl, C. L., Liao, H., Hafner, J. H. *Nano Lett.*, **2006**, *6*, 683.

[55] Grzelczak, M., Perez-Juste, J., Mulvaney, P., Liz-Marzan, L. M. *Chem. Soc. Rev.*, **2008**, *37*, 1783.

[56] Liu, M. P. Guyot-Sionnest. *J. Phys. Chem. B.*, **2005**, *109*, 22192.

[57] Gole, A., Murphy, C.J. *Chem. Mater.*, **2004**, *16*, 3633.

[58] Perez-Juste, J., Pastoriza-Santos. L. M., Liz-Marzan, L. M., Mulvaney, P. *Coord. Chem. Rev.*, **2005**, *249*, 1870.

[59] Ha, T. H., Koo, H. J., Chung, B. H. *J. Phys. Chem. C*. **2007**, 111, 1123.

[60] Millstone, J. E.; Wei, W.; Jones, M. R.; Yoo, H.; Mirkin, C. A. *Nano Lett*. **2008**, *8*, 2526.

[61] Smith, D. K., Miller, N., Korgel, B. A. *Langmuir*, **2009**, *25*, 9518.

[62] Gou, L., Murphy, C. J. *Chem. Mater.*, **2005,** *17,* 3668.

[63] Millstone, J. E., Hurst, S. J., Metraux, G. S., Cutler, J. I., Mirkin ,C. A. *Small*, **2009**, *5*, 646.

[64] Yu, C., Varghese, L., Irudayaraj, J. *Langmuir* **2007,** *23,* 9114.

[65] Takahashi, H., Niidome, Y., Niidome, T., Kaneko, K., Kawasaki, H., Yamada, S. *Langmuir* **2006,** *22,* 2.

[66] Connor, E. E., Mwamuka, J., Gole, A., Murphy, C. J., Wyatt M. D. *Small*, **2005**, *1***,** 325.

[67] Cortesi, R., Esposito, E., Menegatti, E., Gambari, R., Nastruzzi, C. *Int. J. Pharm.*, **1996**, *139***,** 69.

[68] Mirska, D., Schirmer, K., Funari, S. S., Langner, A., Dobner, B., Brezesinski, G. *Colloids Surf. B*, **2005**, *40***,** 51.

[69] Lozano, N., Al-Jamal, W. T., Taruttis, A., Beziere, N., Burton, N. C., Van den Bossche, J., Mazza, M., Herzog, E., Ntziachristos, V., Kostarelos**,** K. *J. Am. Chem. Soc.*, **2012**, *134*, 13256.

[70] Zhang, W., Qiao, X., Chen, J. *Mat. Sci. Eng. B,* **2007**, *142*, 1.

[71] Wijaya, A., Schaffer, S. B., Pallares, I. G., Hamad-Schifferli, K. *ACS Nano*, **2009**, *3*, 80.

[72] Huang, X., Jain, P. K., El-Sayed, I. H., El-Sayed, M. A. *Lasers in Medical Science* **2008**, *23*, 217.

[73] Sarkar, P. K., Chaudhary, A. K. *J. Sci. Ind. Res.*, **2010**, *69*, 901.

[74] H. Tait (ed.), *Five thousand years of glass* (London, The British Museum Press, 1991)

[75] Neetu, S., Anand, C. *Int. J. Res. Pharm.*, **2012**, *3*, 5.

[76] Frens, G. *Nature* 1973, *241*, 20.

[77] Turkevich, J., Hillier, J., Stevenson, P. C. *Disc. Farad. Soc.* **1951**, *11*, 55.

[78] Wilcoxon, J. P., Williamson, R. L., Baughman, R. *J. Chem. Phys.* **1993**, *98*, 9933.

[79] Brust, M., Walker, M., Bethell, D., Schiffrin, D. J., Whyman, R. *J. Chem. Soc., Chem. Commun.* **1994**, 801.

[80] Schutt, E. G. Eur. Patent Application 90317671.4, filed September 25, 1990.

[81] Brown, K. R., Walter, D. G., Natan, M. J. *Chem. Mater*. **2000**, *12*, 306.

[82] Lawn, R. J., Brun, W. A. *Crop Sci.*, **1974**, *14*, 11.

[83] Yamabe, S., Kaneko, K., Inoue, H., Takita, T. *Biosci. Biotechnol. Biochem.*, **2004**, *68*, 250.

[84] Chan, J. M., Zhang, L., Yuet, K. P., Liao, G., Rhee, J., Langer, R., Farokhzad, O. C. *Biomaterials*, **2009**, *30*, 1627.

[85] Morse, W.J. *Yearbook of agriculture,* **1918**, USDA, Washington, D.C., 101.

[86] Makoto Suzuki, M.D., Bradley J. Willcox, M.D., and D. Craig Willcox, Ph.D. "The Okinawa Centenarian Study," **1997,** http://okicent.org/study.html.

[87] Tanito, M., Brush, R. S., Elliott, M. H., Wicker, L. D., Henry, K. R., Anderson, R. E. *J. Lipid Res.*, **2009**, *50*, 807.

[88] Smithers, L. G., Gibson, R. A., McPhee, A., Makrides, M. *Am J Clin Nutr*, **2008,** *88*, 1049.

[89] Quella, S. K., Loprinzi, C. L., Barton, D. L., Knost, J. A., Sloan, J. A., LaVasseur, B. I., Swan, D., Krupp, K. R., Miller, K. D., Novotny, P. J., *J. Clin. Onc.*, **2000**, *18*, 1068.

[90] Clarkson, T. B., *J. Nutr.*, **2002**, *132*, 5665.

[91] Guetta, V., Quyyumi, A. A., Prasad, A., Panza, J. A., Waclawiw, M., Cannon, R. O. III *Circulation*, **1997***, 96*, 2795.

[92] Palmer, R. M. J., Ferrige, A. G., Moncada, S. *Nature*, **1987**, *327*, 524.

[93] Vaz, C., van Doeveren, P. F. N. M., Reis, R. L., Cunha, A. M. *Biomacromolecules*, **2003**, *4*, 1520.

[94] Zema, L., Loreti, G., Melocchi, A., Maroni, A., Gazzaniga, A. *J. Control Release*, **2012**, *159*, 324.

[95] Abdekhodaie, M. J., Liu, Z., Erhan, S. Z. and Wu, X. Y., *Polym. Int.*, **2012** , DOI 10.1002/pi.4244

[96] Silva, S. S., Santos, M. I., Coutinho, O. P., Mano, J. F., Reis, R. L. *J. Mater. Sci. Mater. Med.*, **2005**, *16*, 575.

[97] Henglein, A. *J. Phys. Chem.* **1993**, *97*, 8457.

[98] Henglein, A. *Chem. Rev.* **1989**, *89*, 1861.

[99] Alivisatos, A. P. *J. Phys. Chem.* **1996**, *100*, 13226.

[100] Schmid, G. *Clusters Colloids: From Theory to Application*, VCH: Weinheim, 1994.

[101] Papavassiliou, G. C. *Prog. Solid State Chem.* **1980**, *12*, 185.

[102] Perenboom, J. A. A. J., Wyder, P., Meier, P. *Phys. Rep.* **1981**, *78*, 173.

[103] Hughes, A. E., Jain, S. C. *Adv. Phys.* **1979**, *28*, 717.

[104] Kerker, M. *The Scattering of Light and Other Electromagnetic Radiation*, Academic Press: New York, 1969.

[105] Bohren, C. F., Huffman, D. R. *Absorption and Scattering of Light by Small Particles*, Wiley: New York, 1983.

[106] Creighton, J. A., Eadon, D. G. *J. Chem. Soc., Faraday Trans.* **1991**, *87*, 3881.

[107] Mulvaney, P. *Langmuir* **1996**, *12*, 788.

[108] Brus, L. E. *Appl. Phys. A* **1991**, *53*, 465.

[109] C. J. Murphy. Nanocubes and Nanoboxes. Science, 298:2139–2141, **2002**.

[110] National Institute of Health http://publications.nigms.nih.gov/chemhealth/cool.htm

[111] Finkelstein, N.P., Hancock, R.D. *Gold Bull*., **1974,** *7*, 72.

[112] R. J. Puddephatt. The Chemistry of Gold. Elsevier, **1978**.

[113] Baschand, H., Gray, H.B. *Inorg. Chem.*, **1967,** *6*, 365.

[114] Miessler, G. L., Tarr, D. A. *Inorganic Chemistry,* 4th ed., Prentice Hall: Upper Saddle River, 2011.

[115] Mason, W.R., Gray, H.B. *J. Am. Chem. Soc*., **1968**, *90*, 5721.

[116] Eustis, S. PhD. Dissertation, Georgia Institute of Technology, 2006.

[117] D. J. Shaw. Introduction to Colloid and Surface Chemistry. Butterworths, 3rd edition, **1989**.

[118] H.-F. Eicke. Modern Trends of Colloid Science in Chemistry and Biology, Birkhäuser Verlag, Basel, **1985**.

[119] Mie, G. *Annalen Der Physik*, **1908**, *25*, 377.

[120] U. Kreibig and M. Vollmer. *Optical Properties of Metal Clusters*, **1995**, *25*. Springer, Berlin.

[121] C. F. Bohren and D. R. Huffman. *Absorption and Scattering of Light by Small Particles*. **1983**, Wiley, New York.

[122] C. Kittel. *Introduction to Solid State Physics.* **1966**, John Wiley & Sons, Inc., third edition.

[123] R. E. Dodd. *Chemical Spectroscopy*. **1962**, Elsevier, New York.

[124] Mulvaney, P. *Langmuir*, **1996**, *12*, 788.

[125] Link, S., El-Sayed, M.A. *J. Phys. Chem. B*, **1999**, *103*, 4212.

[126] Kreibig, U., Fragstein, C.V. *Z. Phys.*, **1969**, *224*, 307.

[127] van der Zande, B.M.I., Böhmer, M.R., Fokkink, L.G.J., Schönenberger, C. *Langmuir*, **2000**, *16*, 451.

[128] Gans, R. *Annalen Der Physik*, **1912**, *37*, 881.

[129] Zheng, J., Zhang, C., Dickson, R.M. *Phys. Rev. Lett.*, **2004**, *93*, 077402.

[130] Link, S., El-Sayed, M.A. *J. Phys. Chem. B*, **1999**, *103*, 3073.

[131] Link, S., El-Sayed, M.A. *J. Phys. Chem. B*, **1999**, *103*, 8410.

[132] Nikoobakht, B., El-Sayed, M.A. *Chem. Mater.*, **2003**, *15*, 1957.

[133] Percz-Juste, J., Pastoriza-Santos, I., Liz-Marzán, L. M., Mulvaney, P. *Coord. Chem. Rev.*, **2005**, *249*, 1870.

[134] Yu, C., Varghese, L., Irudayaraj, J. *Langmuir* **2007,** *23,* 9114.

[135] Nune, S., Chanda, N., Shukla, R., Katti, K., Kulkarni, R. R., Thilakavathy, S., Mekapothula, S., Kannan, R., Katti, K. *J. Mater. Chem.*, **2009**, *19*, 2912.

[136] Markowitz, M.A., Dunn, D.N., Chow, G.M., Zhang, J. *J. Colloid Interface Sci.* **1999**, *210*, 73.

[137] Pileni, M.P. *Nat. Mat.*, **2003**, *2*, 145.

[138] Regev, O., Backov, R., Faure, C. *Chem. Mater.*, **2004**, *16*, 5280.

[139] A. Bose, J. Sarkar Nanostructured Materials for Advanced Transportation Applications. Report to University of Rhode Island, URITC Project No. 000464, Kingston, RI 02881, 2001.

[140] Bell, F. P. *Prog. Lipid Res.*, **1978**, *7*, 207.

[141] Dawidowicz, E. A. *Curro Top. Membr. Transp.,* **1987**, *29*, 175.

[142] Kaplan, M. R ., Simoni, R. D. *Cell Bioi.*, **1985**, *101*, 441.

[143] Kaplan, M. R ., Simoni, R. D. *Cell Bioi.*, **1985**, *101*, 446.

[144] Vance, E. *Biochim. Biophys. Acta.,* **1988**, *963*, 10.

[145] Wirtz, K. W. A. *Annu. Rev. Biochem.*, **1991**, *60*, 73.

[146] Alper, J., Hamad-Schifferli, K. *Langmuir*, **2010**, *26*, 3786.

[147] Chithrani, B. D., Ghazani, A. A., Chan, W. C. W. *Nano Lett.*, **2006**, *6*, 662.

[148] Dai, Q., Coutts, J., Zou, J., Huo, Q. *Chem. Commun.*, **2008**, *44*, 2858.

[149] Hiramatsu, H., Osterloh, F. E. *Chem. Mater.*, **2004**, *16*, 2509.

[150] Chen, H. M., Liu, R., Asakura, K., Jang, L., Lee, J. *J. Phys. Chem. C*, **2007**, *111*, 18550.

[151] Johnson, C. J., Dujardin, E., Davis, S. A., Murphy, C. J., Mann, S. *J. Mater. Chem.* **2002**, *12*, 1765.

[152] Yu, C. X., Varghese, L., Irudayaraj, J. Langmuir, **2007**, *23*, 9114.

[153] Dai, Q., Coutts, J., Zou, J., Huo, Q. *Chem. Commun.*, **2008**, *25*, 2858.

[154] Huang, X., El-Sayed, I. H., Qian, W., El-Sayed, M. A. J. Am. Chem. Soc., **2006**, *128*, 2115.

[155] Jie An Yang, J., Murphy, C.J. *Langmuir*, **2012**, *28*, 5404.

[156] Lofton, C., Sigmund W. *Adv. Funct. Mater.*, **2005**, *15*, 1197.

[157] a) Kryndushkin D. S., Alexandrov I. M., Ter-Avanesyan M. D., Kushnirov V. V.

Journal of Biological Chemistry, **2003**, *278*, 49636. b) J. Sambrook, D. W. Russel Molecular Cloning: A Laboratory Manual *3rd Ed*. Cold Spring Harbor Laboratory Press. Cold Spring Harbor, NY., 2001. c) J. M. Berg, J. L. Tymoczko, L. Stryer Biochemistry *5th ed.* WH Freeman, 2002.

[158] Hanauer, M., Pierrat, S., Zins, I., Lotz, A., Sönnichsen, C. *Nano Lett.*, **2007**, *7*, 2881.

[159] Habashi, F. Recent Advances in Gold Metallurgy, *Revisa de la Facultad de Ingeniera, Universidad Central de Venezuela* **1998**, *13*, 43.

[160] Mackiewicz, M. R., Ayres, B. R., Reed, S.M. *Nanotechnology*, **2008**, *19*, 115607.

[161] Loftus, A. F., Reighard, K. P., Kapourales, S. A., Leopold, M. C. *J. Am. Chem. Soc.*, **2008**, *130*, 1649.

[162] Fan, H., Leve, E. W., Scullin, C., Gabaldon, J., Tallant, D., Bunge, S., Boyle, T., Wilson, M. C., Brinker, C. J. *Nano Lett.*, **2005**, *5*, 645.

[163] a) Daniel, M. Astruc, D. *Chem. Rev.*, **2004**, *104*, 293. b) Paulini, R., Frankamp, B. L., Rotello, V. M. *Langmuir*, **2002**, *18*, 2368**.**

[164] a) Plant, A. *Langmuir*, **1999**, *15*, 5128, b) Brevnov, D. A., Finklea, H.O. *Langmuir*, **2000**, *16*, 5973.

[165] a) Cornell, B. A., Braach-Maksvytis, V. L. B., King, L. G., Osman, P. D. J., Raguse, B., Wieczorek, L., Pace, R. J. *Nature*, **1997**, *387*, 580, b) He, L., Robertson, J. W. F., Li, J., Kärcher, I., Schiller, S. M., Knoll, W., Naumann, R. *Langmuir*, **2005**, *21*, 11666, c) Köper, I. *Mol. BioSyst.*, **2007,** *3*, 651.

[166] a) Sitaula, S., Mackiewicz, M. R., Reed, S. M. *Chem. Commun*., **2008**, *44*, 3013. b) Jana, N. R., Gearheart, L., Obare, S. O., Murphy, C. J. *Langmuir*, **2002**, *18*, 922. c) Rodr´ıguez-Ferna´ndez, J., Pe´rez-Juste, J., Mulv- aney, P., Liz-Marza´n, L. M. *J. Phys. Chem. B*, **2005**, *109*, 14257.

[167] Szule, J. A., Fuller, N. L., Rand, R. P. *Biophys. J.,* **2002**, *83*, 977.

[168] Zimmerberg, J., Kozlov, M. M. *Nat. Rev. Mol. Cell Biol.*, **2006**, *7*, 9.